

**Anatomic Characterization and Profilometry of Tissues with
Natural Shape: A Real-time Approach for Robotic-Assisted
Minimally Invasive Surgery**

A Thesis

In

The Department

Of

Mechanical & Industrial Engineering

Presented in Partial Fulfillment of the Requirements

For the Degree of Master of Applied Science at Concordia University

Montreal, Quebec, Canada

December 2015

©Ali Reza HASSAN BEIGLOU, 2015

CONCORDIA UNIVERSITY

School of Graduate Studies

This is to certify that the thesis prepared

By: Ali Reza HASSAN BEIGLOU

Entitled: Anatomic characterization and profilometry of tissues with natural shape: a real-time approach for robotic-assisted minimally invasive surgery

And submitted in partial fulfillment of the requirements for the degree of

Master of Applied Science (Mechanical Engineering)

Complies with the regulations of the University and meets the accepted standards with respect to originality and quality.

Signed by the final examining committee:

__ Dr. Rajamohan Ganesan _____ Chair

__ Dr. Xie, Wen-Fang _____ Examiner

__ Dr. Hassan Rivaz _____ Examiner

__ Dr. Javad Dargahi _____ Supervisor

Approved by:

Chair of Department or Graduate Program Director

Abstract

Ali Reza HASSAN BEIGLOU

Concordia University, 2015

This master thesis is divided into two major sections. First, anatomic characterization and profilometry of tissues with natural shape: a real-time approach for robotic-assisted minimally invasive surgery (RMIS); and second, design and characterization of a novel tactile array sensor capable of differentiating among different viscoelastic tissues that exhibit time-dependent behaviour.

The first part of this thesis is focused on a tissue characterization system for RMIS applications. RMIS has gained immense popularity with the advent of high-precision robotic systems. The lack of haptic feedback, however, is considered as being one of the main drawbacks of present-day RMIS systems. In order to compensate for this deficiency, a novel tissue characterization system is proposed which is inspired from the human haptic system. Hence, kinesthetic and tactile feedback which are constitutive components of human haptic system are used to characterize naturally shaped tissues. Toward this goal, a 5-degree-of-freedom robot which is called Catalys5 is equipped with a ball caster force-cell. The system is used to simulate robotic surgery maneuvers in which an admittance control approach is implemented to design the force feedback controller. The proposed method characterizes naturally shaped tissues, which is capable of touching and palpating to: a) Identify the 2D or 3D surface profile of the target tissue (profilometry), b) Measure the modulus of elasticity of any desired point on the tissue's surface, c) Find and map the location of any lump in the tissue, and d) Map hardness distribution around the lump.

Initially, silicon-rubber materials were used to build tissue phantoms with different curvatures and degrees of softness. The surface profiles were obtained using the developed profilometry algorithm and validated using a 3D scanner. In addition, several experiments were conducted on bovine tissues to evaluate all above mentioned capabilities of the system. The results of experiments on real tissues were also compared to those that are available in current literature.

The results indicate that the proposed approach can be used for reliable material characterization for RMIS application.

The second part of this thesis is focused on developing an array tactile sensor for distinguishing softness of viscoelastic tissues with time-dependent behaviour for use in MIS and RMIS. Review of literature on tactile sensors reveals that the vast majority deals with determining the applied contact force and object elasticity. In this research, a novel idea is proposed in which a tactile sensor array can measure rate of displacement in addition to force and displacement of any viscoelastic material during the course of a single touch. In order to verify this new array sensor, several experiments were conducted on a range of biological tissues. It was concluded that this novel tactile sensor can distinguish among the softness of real biological tissue with time-dependent behaviour.

Acknowledgment

This research would not be possible without the help and guidance of several people. Primarily, I would like to thank my supervisor, Dr. Javad Dargahi for his remarkable ideas, encouragement, guidance and constant support. I particularly appreciated the freedom he accorded to my research, and the trust he placed in my capabilities. He always encouraged my steps from the very beginning of my studies in Canada, even before I officially began my program in Concordia University.

I would like to thank my friends who helped me throughout my master's program: Ali Fella Jahromi, Masoud Kalantari, Siamak Arbatani, Shahram Shokouhfar, Ehsan Zahedi, and Mostapha Marzban. I learned from their technical experience and management skill.

Also, I would like to thank my colleagues and friends who helped and accompanied me along my master's program: Zahra Rostamkhani, Masoud Ali, Hossein Khodadadi, Mohammad Khosravi, Roozbeh Shams, Mohammad Keshmiri, Alexandre Laroche, Mohsen Tayefeh, Amir Hooshir and Masoud Razban.

Robotic minimally invasive surgery requires heavy collaboration and interdisciplinary experience. I would therefore like thank Concordia's technicians and friends who gracefully shared their resources and know-how: Gilles Huard, Robert Oliver, Tianhe Wen, Dan Juras, Andrzej Krysztofowicz and Arash Fella Jahromi.

Additionally, I would to thank Dr. Luca Caminati and Mary Appezzato who guided me in preparation and arrangement of my thesis according to Concordia University's requirements.

I would also like to thank the administrative staff at Concordia University: Arlene Zimmerman, Leslie Hossien, Sophie Mrineau, Maureen Thuringer, and Charlene Wald.

My deepest heartfelt gratitude goes out to my wife, Shila Norouzi. Her support and encouragement were felt from the very beginning step of my study in Canada. Without her support, I would not have been able to accomplish this thesis. I would also like to express my profound gratitude to my father Gholamreza, my mother Maliheh, my sister Samaneh and my brother Mohammadreza. Their boundless love and dedication have been an inspiration

throughout my life. Words simply cannot express the love I have for my family. They have been with me every step of the way and I could not have achieved much without them.

Finally, I would like thank Concordia University and its staff for providing me with the opportunity to carry out my studies at the master's level

Contributions of authors

The thesis is presented in manuscript-based format in four chapters. The thesis consists of three journal papers: two have been published, and the last one has been submitted for publication. The first two papers are contributions of the author. Chapter 2 covers the content of these papers in detail.

The citations for these journal papers are as follows:

- 1- Ali Reza HASSAN BEIGLOU, and Javad Dargahi. "Real-Time 2D Surface Profile Mapping of Biological Tissue with Force Feedback in Robot-Assisted Minimally Invasive Surgery". *Applied Mechanics and Materials*, vol. 798, pp. 319-323. Trans Tech Publications, 2015.
- 2- Hassanbeiglou, A. and Dargahi, J. "Anatomic Characterization and Profilometry of Tissues with Natural Shape: A Real-time Approach for Robotic-Assisted Minimally Invasive Surgery". is submitted in *Medical Image Analysis Journal*.
- 3- Hassanbeiglou, Alireza, Masoud Kalantari, Elaheh Mozaffari, Javad Dargahi, and József Kövecses. "A New Tactile Array Sensor for Viscoelastic Tissues with Time-Dependent Behavior." *Sensor Review* 35, no. 4 (2015): 374-381.

In Chapter 3, the novel design and characterization of an array tactile sensor based on piezoresistive sensing element is presented. The sensor was designed and initial testing was performed by Dr. Kalantari in chapter 5 of his PhD thesis. In chapter 3 of this thesis the author further developed the fabrication of the sensor. In addition, more in-depth literature review was conducted. Furthermore, addition new experiment of work was done specially on real bovine tissues. The author has conducted analysis and discussion of the new results. Contribution of Dr. Mozaffari was to assist in the development of Labview simulation.

Table of Contents

Chapter 1 – Introduction	1
1.1 Problem and Motivation.....	1
1.1.1 Anatomic characterization and profilometry of tissues with natural shape: a real-time approach for robotic-assisted minimally invasive surgery	2
1.1.2 A new tactile array sensor for viscoelastic tissues with time-dependent behavior... 3	
1.2 Thesis Outline	4
Chapter 2 - Anatomic characterization and profilometry of tissues with natural shape: a real-time approach for robotic-assisted minimally invasive surgery	6
2.1 Introduction	6
2.1.1 Characterizing tissue with imaging techniques.....	7
2.1.2 Tissue characterization in RMIS using tactile sensors	8
2.2 Methodology	10
2.2.1 Manipulator with force feedback	14
2.2.2 Profilometry of organ with natural shape	19
2.2.3 Tissue characterization system and surface profile display	28
2.2.4 Tissue stiffness calculation based on characterized contact	32
2.3 Result, discussion and performance analysis	34
Chapter 3 - A new tactile array sensor for viscoelastic tissues with time-dependent behavior....	47
3.1 Introduction	47
3.2 Sensor Structure Design.....	50
3.3 Sensor Fabrication.....	51
3.4 Sensing Algorithm.....	53
3.5 Experiments.....	56
Chapter 4 - Conclusion and future work.....	64

List of Figures

Figure 1. Robotic assisted minimally invasive surgery system	1
Figure 2. Lindbergh operation, the first medical history of tele surgery operation, which was operated on a patient on Strasbourg by the surgeon team in New York	2
Figure 3. Experiment Setup, 5 DOFs Robot, Ball caster Force Sensor and Silicon Rubber material	9
Figure 4. Material characterization system block diagram.....	13
Figure 5. Distributing the real-time calculations on three PCs.....	14
Figure 6. Force sensor element including ball caster, strain gauge and Phidget Bridge	16
Figure 7. Admittance control approach	17
Figure 8. FFC stabling force on surface of material with 32 KPa (red line) and 0.8 KPa (blue line) elasticity modulus.....	17
Figure 9. Robot 2D maneuver with FFC	18
Figure 10. (a) Passing on bumpy surface (b) Steady state error of the FFC in force stabilization during the passed distance	19
Figure 11. Produced X and Y trajectory to be followed by the robot, (a) Radius: 40mm, distance between nodes: 5mm (b) Radius: 10mm, distance between nodes: 2.5mm	21
Figure 12. (a) Scanned and real surface of the tissue, each segmented color represents the real corresponding surface of the same color (b) Translational movement on $b'c'$ which is saved as bc1 (c) Passing the ball caster on a sharp edge, the blue circle is tangent to the AI and the gray circle is tangent to IB. Point I is the center of $C1C2C3$	22
Figure 13. (a) Elliptical shape built by silicon rubber material Ecoflex 00-10 ($E= 0.8$ KPa) (b) 2D STA transformation for specimen shown in (a). Each blue circle on scanned surface is transformed by TSA from the scanned surface.....	23
Figure 14. (a) Spherical shape specimen which is made of Ecoflex 00-10 0.8 KPa	24
Figure 15. (a) Built elliptical silicon rubber (Ecoflex 00-10 base softened with silicon oil) (b) Scanned elliptical material with ball caster	25

Figure 16. (a) Scanned surfaces with rolling ball and 3D scanner (b) Iterative closest point algorithm result, the scanned cloud by the 3D scanner is considered as reference (c) Root Mean Square error which is calculated for each iteration.....	27
Figure 17. (a) Indented spherical ball on a tissue with curvature surface (b) Contact boundary points of the indented ball and nonplanar tissue (c) Enlarged contact area (d) Indented ball on surface of Ecoflex 00-10 (e) Detected points of contact for the moment which is shown in (d) .	29
Figure 18. (a) Detected contact points on surface (b) Fitted circle on detected contact points (c) Detected contact point on lower hemisphere of ball which is indented on surface of material (d) Imaginary circular surface in contact area	32
Figure 19. (a) Spherical indenter on spherical surface (b) Inclined indentation on material surface, F_s is measured by stain gauge and the n is the normal interaction of surface.....	33
Figure 20. (a) Bovine liver (b) 3D scanned surface profile of the liver (c) Bovine kidney (d) 3D scanned surface profile of kidney (e) Bovine heart (f) 3D scanned surface profile of the heart ..	35
Figure 21. 2D Scanned surface profile of (a) Liver (b) Kidney (c) Heart	37
Figure 22. Captured force (F_n) versus measured effective indentation (i) on liver tissue in spot selection, 2D and 3D mode for points (a) l_1 and l_4 (b) l_2 and l_4 (c) l_3 and l_4	41
Figure 23. Captured force (F_n) versus measured effective indentation (i) on liver tissue in spot selection, 2D and 3D mode for points (a) h_1 and h_4 (b) h_2 and h_5 (c) h_3 and h_6	43
Figure 24. (a) Artificial plastic lumps which are buried in depth of 20 mm from tissue surface (b) 100mm pre-defined maneuver for lump detection (c) Calculated elasticity modulus of tissue which is selected by 2.5 mm distance for the lump detection	46
Figure 25. (a) Schematic exploded view of the sensor and its components	51
Figure 26. (a) Components of array sensor (b) The fabricated array sensor size	52
Figure 27. (a) Manufactured components of the array tactile sensor (b) Fabricated tactile Sensor	53
Figure 28. Sensing flowchart for tactile sensor	54
Figure 29. Equipment used to test the tactile sensor array	56
Figure 30. Progressive indentation of the tactile sensor into the tissue	57
Figure 31. Force-displacement response of tissue 1 (atrial) for different rates	58
Figure 32. Comparison of the measured force of the array sensor and ElectroForce Bose 3200 for tissue 1 with an indentation rate of 0.1 mm/s	59

Figure 33. Comparison of measured force of array sensor and ElectroForce Bose 3200 for tissue 1 with indentation rate of 10 mm/s	59
Figure 34. Result of tactile sensor on three tissues at an indentation rate of 0.1 mm/s	60
Figure 35. Result of tactile sensor on three tissues for 1 and 10 mm/s indentation rates	61
Figure 36. Regeneration flow chart of softness for nonlinear materials.....	63

List of Tables

Table 1. Steady state error of FFC for the touched length shown in Figure 6. (a)	19
Table 2. Elasticity modulus calculated in spot selection mode	36
Table 3. Material characterization in 2D mode	38
Table 4. Material characterization result for 3D mode	40
Table 5. Modulus of elasticity for bovine liver and kidney in literature	44
Table 6. Tissue types and dimensions.....	56

List of Equations

Equation 1. Dynamic of robot which interact with external environment.....	15
Equation 2. Archimedean spiral equation.....	19
Equation 3. 2D transformation	22
Equation 4. 3D transformation.....	23
Equation 5. Indentation on surface.....	28
Equation 6. Depth calculation of two intersected surfaces	32
Equation 7. Effective radius of two intersected surfaces	32
Equation 8. Elasticity modulus of indented tissue.....	33
Equation 9. Average displacement rate of sensor.....	54

Chapter 1 – Introduction

1.1 Problem and Motivation

Minimally invasive surgery (MIS) has brought significant advantages to surgical tasks [1]. This method allows surgeons to perform operations without direct access to patient's body. Recent robotic developments have made possible to integrate the conventional MIS with robotic systems. Result of this integration is robotic assisted minimally invasive surgery (RMIS) [2, 3], in which the surgeon conducts the task through master part of the system. The tasks to be followed by slave part, where the patient is located as it is shown in Figure 1. The RMIS system provides remarkable accuracy and dexterity for surgeons [4]. The operation can be performed through a small cut. As a result, decreasing trauma for the patients along with reducing hospitalization cost can be enumerated as the main advantages of the RMIS [5, 6].

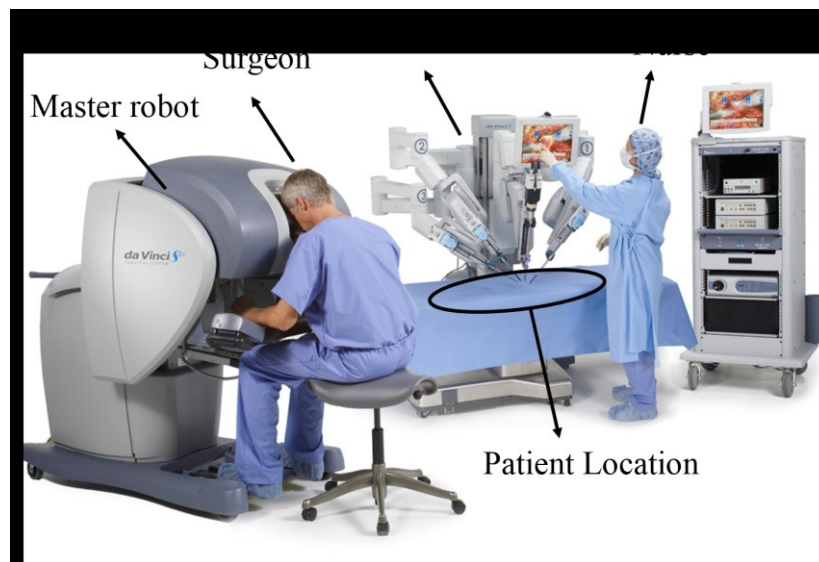


Figure 1. Robotic assisted minimally invasive surgery system [7]

Efficient achievement in field of high speed network during last decade enables the surgeons to execute the complicated RMIS operation remotely over high speed networks. For example, Lindbergh operation [2] was first complete tele operation surgery, which is done by surgeons located in New York on a patient in Strasbourg in France (Figure 2).

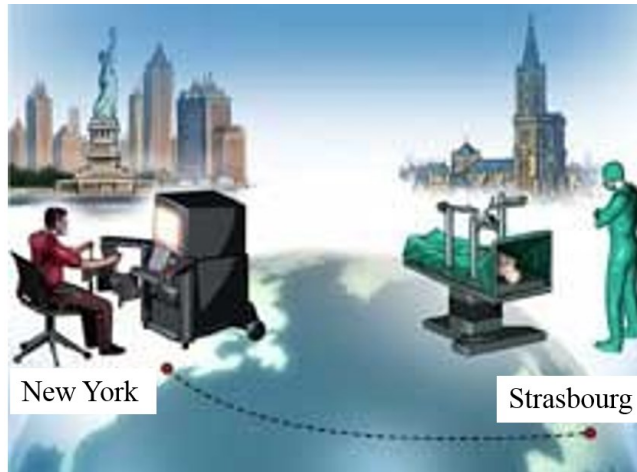


Figure 2. Lindbergh operation, the first medical history of tele surgery operation, which was operated on a patient on Strasbourg by the surgeon team in New York [8]

The haptic feedback information in open surgery is transferred to surgeon's brain with direct touching and palpating of tissues in surgical field. In RMIS operation the surgeon doesn't have direct access to the tissues. As a result, the surgeon loses sense of touch which plays an important rule during the surgery. Through this crucial sense the surgeon is able to get mechanical properties of tissue such as softness and even abnormality of tissue in terms of softness (elasticity modulus). Lack of haptic feedback [9] which is caused from nature of master-slave robotic manipulation is still considered as the main drawback of RMIS. The current research has two main goals, which are directly related to mentioned deficiency of RMIS systems. 1- To develop a novel tissue characterization and profilometry system are proposed for RMIS system, which characterizes the tissue real-time. 2- To develop a sensor for viscoelastic material with time-dependent response, which can be used a tactile sensor in MIS and RMIS applications.

1.1.1 Anatomic characterization and profilometry of tissues with natural shape: a real-time approach for robotic-assisted minimally invasive surgery

In the first part of this thesis, a novel tissue characterization and profilometry system are proposed for RMIS systems. The proposed method is inspired from human touch system. Constitutive components of human haptic systems in which "kinesthetic" and "tactile" feedbacks

were recreated to design the artificial haptic system. The knowledge of human motor control, materials science, biological tissue, surface metrology, robotics, and controls were used to develop the proposed method of artificial human haptic system.

Information such as 3D shape, softness, and relative hardness of objects touched by the robot could be obtained through a direct touch on the surface of a material. Using the proposed system surface profile, the modulus of elasticity and location of lumps in tissues are displayed for the user. Several experiments were done on silicon rubber phantom for the purpose of design validation. The accuracy of the surface profile capturing function was evaluated using silicon rubber specimens. The captured surfaces were compared to surface profile results from a commercial 3D scanner. The material identification process includes contact detection, depth calculation and a contact characterization algorithm which is discussed in detail in chapter 2.

Several experiments were performed on bovine tissue in order to obtain realistic validation data. Various locations on specimens with local curvatures were evaluated by a material identification module, and the results were compared with those from literature. In the final portion of Chapter 2 it is shown how a fully developed artificial haptic system is capable of finding lumps beneath the surface of a tissue. The system shows abnormalities of the tissue in terms of (relative) softness on a captured surface profile.

1.1.2 A new tactile array sensor for viscoelastic tissues with time-dependent behavior

Second part of this thesis is related to design and characterization of a tactile array sensor which can distinguish among biological viscoelastic tissues with time-dependent behaviour. The viscoelastic model of a tissue is the most realistic representation of its mechanical behavior, and that of live tissues. The proposed sensor measures the capture force during indentation tests on a material with viscoelastic properties. The captured force is analyzed in a sensing algorithm, which saves the contact force between the surface of a tissue and the sensor. The proposed sensor can be considered as a new generation of tactile sensor because it extracts the indentation depth and displacement rate in addition to force and displacement. This capability can be beneficial in other applications; such as for use in robotic arms and humanoid robots. The trapezoidal shape of the sensor enables the algorithm to measure average displacement rate (average velocity) during a single touch. Several indentation tests were done on bovine tissues.

The results indicate that the developed sensor can reliably differentiate between biological tissues with viscoelastic behaviour.

1.2 Thesis Outline

The rest of the thesis is structured as follows:

Chapter 2 - Anatomic characterization and profilometry of tissues with natural shape: a real-time approach for robotic-assisted minimally invasive surgery

The concept of a master slave robot, RMIS and associated problems of MIS and RMIS methods are described. A comprehensive literature review is summarized, in which existing methods are presented in the context of the measurement of mechanical properties of tissues during RMIS.

Section 2.2 describes the control approach of robots, surface profile, contact detection and calculation of tissue stiffness. They are discussed in detail as sub-algorithms of artificial haptic systems.

The results, discussion and performance analysis is discussed in section 2.3. The elastic modulus, which was calculated using the proposed method, is compared with those found in literature. The system can be used for abnormality detection in biological tissue with respect to relative softness.

Chapter 3 - A new tactile array sensor for viscoelastic tissues with time-dependent behavior

Design and characterization of a new tactile sensor for MIS and RMIS applications is presented. In Section 3.1, the applications of the proposed sensor are discussed. It can be used as a non-invasive probe for cancer detection, in a humanoid robot, or during MIS and RMIS. The literature review on similar tactile sensors is also discussed.

In Section 3.2, the sensor structure design including fabrication and sensing algorithm is discussed. The experiments on biological tissue and discussion on the results are presented in Section 3.3.

Chapter 4 - Conclusion and Future Work

In the beginning of this chapter, the overview of the thesis contributions is presented. The conclusion of the each main part of thesis is discussed in this section. The chapter continues by presenting some opportunities for future research.

Chapter 2 - Anatomic characterization and profilometry of tissues with natural shape: a real-time approach for robotic-assisted minimally invasive surgery

2.1 Introduction

Teleoperation tasks employing the use of master slave systems have been used ever since 1940 [5]. However, it was not until 1985 that the emergence of the Programmable Universal Manipulation Arm (PUMA) revolutionized high precision tele manipulation operations. These accurate motion controllers facilitated vital operations such as Robotic Minimally Invasive Surgery (RMIS)[2] and, along with the progressive developments in robotics and tele manipulation, RMIS became a viable substitute for conventional and Minimally Invasive Surgery (MIS) [1]. Advances in RIMS during the past few years have enabled surgeons to execute the most complicated surgical procedures, including mitral valve repair [10] and pulmonary resection operation [11]. Since the surgeon is now provided with increased dexterity and precise maneuvering during MIRS, only a small incision is now required with corresponding reduced tissue trauma and, therefore, faster recovery time. However, since surgeons still do not have direct access to the patient's body in RMIS, they lose the perception that is afforded to them by direct touching and palpating the tissue [12, 13]. In other words, the lack of haptic feedback [14] , which is caused by the nature of master slave manipulation, is still considered as being one of the main drawbacks in present-day RMIS.

The haptic information, which comes from direct palpating of soft tissues, can be categorized into two groups. First, mapping data that contains information based on the location and shape of the goal tissue in the surgical field. Second, the mechanical properties of soft tissue, which is manifested in terms of (relative) softness. In fact, during open surgery, it is the combination of mapping data and the sense of touch perception provides haptic feedback for surgeon [15]. Studying each constitutive part of human haptic system has led to the development of imaging techniques and tactile sensors in order to provide this lost haptic information during MIRS.

2.1.1 Characterizing tissue with imaging techniques

Although imaging techniques have been used as common methods to provide visual images during surgery for both MIS and open procedures, it was not until researchers combined different imaging techniques that it was possible to obtain the mechanical properties of tissues and locate abnormalities. Hekimoğlu *et al.* demonstrated the combination of three methods, namely T2-weighted, diffusion weighted magnetic MRI and proton magnetic resonance spectroscopy correlated with histopathology which led to recognizing the cancerous tissues within the prostate [16]. Similarly, investigations conducted by Karatopis *et al.* concluded that the combination of magnetic resonance spectroscopy (MRS) and magnetic resonance spectroscopic imaging (MRSI) is capable of localizing, with acceptable spatial resolution, cancerous tissue contained in breast lesions [17]. However, in image guided surgery, the rigid-body approximation is considered as being a main principle whereas the deformation brings uncertainty for using the images, which is prepared prior to the operation, notwithstanding the fact that it is an inevitable characteristic of biological tissue [18]. Furthermore, techniques that are used in real-time MRI, such as those necessary in minimally invasive urology surgery [19], are still limited in scope and versatility not to mention those that are even more demanding in the context of general surgery [20]. On the other hand, although development of a robot that is compatible for use during an MRI procedure is another challenging task [21, 22], some researchers have developed MIS systems for limited types of surgeries which are capable of working within an MRI environment. Stoianovici *et al.* developed a pneumatic step motor made of nonmagnetic and dielectric materials, and fiber optic as the motor encoder [23]. The motor is used to actuate the first MRI compatible robot to perform transperineal percutaneous needle access in radioactive seed implant operations under real-time MRI imaging [24]. Masamune *et al.* proposed a needle insertion manipulator which comprised polyethylene terephthalate that was actuated by ultrasonic motors [25]. However, MRI does impose severe limitations when it comes to manufacturing elements of robotic surgical tools in terms of material selection, design and computability of equipment [26]. It therefore becomes necessary for researchers to develop techniques that provide mechanical characteristics of goal tissue in surgical field using tactile sensors.

2.1.2 Tissue characterization in RMIS using tactile sensors

Soft organs, which are goal tissues in the surgical field, exhibit complex mechanical behavior. This behavior can be studied based on inherent characteristics of biological tissue in terms of nonlinearity [27], anisotropy [28], nonhomogeneity[29], time and rate dependency [30]. Although there are different developed tactile sensors that are capable of obtaining the mechanical properties of soft biological tissues, considering the complex behavior of biological tissues each tactile sensor must be evaluated based on the type and accuracy of parameters which the sensor characterize during sensor/tissue interaction. Samur *et al.* developed a robotic indenter for minimally invasive measurement for pig liver characterization [31]. Their device characterizes the pig liver properties based on nonlinearities resulting from contact, geometry and viscoelastic/hyperelastic material model. Hassanbeiglou *et al.* developed an array sensor that is able to distinguish between soft tissues with viscoelastic behavior for MIRS application. During an indentation test, it was shown how the developed sensor was able to distinguish between different bovine tissues types considering the rate-dependent response of the tissues [32, 33]. Xie *et al.* developed an optical tactile array probe for MIS applications which is able to detect embedded nodules inside soft tissues. In their method, spatial distribution of tactile force feedback detected tissue abnormalities. They demonstrated that the performance of their system provided accurate results when the sensor was used on artificial soft flat surfaces but were inaccurate on non-flat surfaces [34]. Samur *et al.* classified and compared the measurement methods according to the in situ and in vitro context of measurement for tactile sensors [31]. They determined that most of the specimens used in tissue related measurements were excised and well-shaped from the goal tissues. As a result, by knowing the actual dimensions, cross-section and well defined boundary conditions applied to the specimens, different methods of measurement can be easily applied to calculate the mechanical properties of each tissue. However, the ideal choice when requiring the most accurate mechanical characteristic of a tissue would be to test it in its natural state [35].

Based on above, characterization of naturally shaped tissue is the most desirable and accurate approach. Hence, in this research we propose a novel approach which can be applied for in vivo measurement during RMIS. The method was developed to compensate for the lost haptic feedback that is still a shortcoming in current RMIS procedures. The system itself has four different features which enables the surgical robot to:

- a) touch and palpate the tissues without indenting the surface to show the tissue's surface topography (profilometry of tissue),
- b) apply controlled indentation on the tissue surface in order to calculate its modulus of elasticity,
- c) determine the location of buried lumps beneath the surface of a tissue, and
- d) map the hardness distribution around the lump.

In order to simulate robotic surgery, and to evaluate all the above-mentioned capabilities, a test rig was developed as shown in Figure 3. The experimental set-up included a 5 degree of freedoms (DOFs) robot as the slave part of the robotic surgical instrument, fabricated silicon rubber materials as the goal tissues, different sizes of balls (buried in the rubber as artificial lumps) and a strain gauge force cell with ball caster tip. The spherical ball, which interacts with the material, produces less stress concentration on the surface under investigation and can move over the material surface.

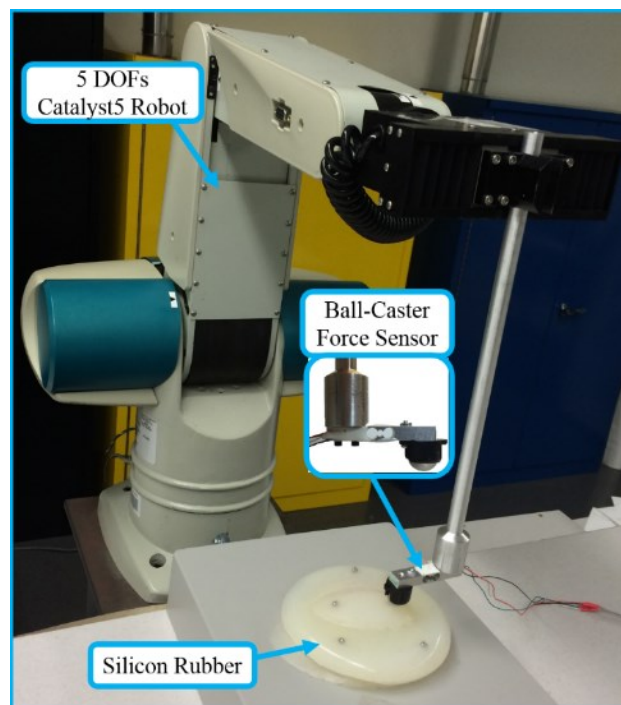


Figure 3. Experiment Setup, 5 DOFs Robot, Ball caster Force Sensor and Silicon Rubber material

2.2 Methodology

The purpose of this research is to design and develop a novel method which compensates for the lost haptic feedback which, as previously mentioned, is the major drawback of current RMIS procedures. The human haptic perception, together with its constituent components, were used as an inspiration to design the proposed method. In the human haptic system, when a material is touched, sensory receptor impulses on the skin and characterizes its size, shape and texture by providing kinesthetic and cutaneous feedback sensing to the brain.

Firstly, kinesthetic feedback [36] helps to provide information based on the geometry [37], shape [38, 39], and weight [40] of any object touched by the hands. All the feedback from receptors embedded in muscles, joints and tendons carry the signals to brain, which is able to calculate the position, shape and geometry of object. Playing a musical instrument is one of most dexterous operations which uses this kind of joint and sensory feedback [41]. This human phenomena is used to add kinesthetic feedback algorithm for the robotic system which consists of a 5 DOFs serial manipulator called Catalyst-5 that operates as the slave part in robotic surgery. When the end-effector of a robot grips or touches a point in the global XYZ coordination on the robot base, forward kinematics of the robot can calculate the precise relative position of the touched object with regard to the reference coordinate of the robot [42]. This operation is made possible by the encoders that are installed in each joint of the robot since, by knowing the boundary points of the touched object, the shape can be shown in the robot's coordination system. This shape is similar to the 3D concept that forms in the human brain after touching. The procedure detailing the robot touching the goal tissue without indenting the surface is described in section 2.2.1.2.

Secondly, tactile sensing is the other part of human haptic feedback in which the skin mechanoreceptors are fundamental sensory receptors that respond to pressure and deformation [43]. During a single touch, the brain actively processes this tactile feedback received from mechanoreceptors [6]. The touching procedure for soft tissues is accompanied with indenting the object. As the depth of touch increases, the intensity of the reaction force inherent within the material increases causing the mechanoreceptors to detect a correspondingly larger force [44]. The combination of this tactile force and kinesthetic feedback, previously discussed, informs the human about the direction of stress [45] which is the same as the normal vector plane of the two interfered surfaces [46]. The latter direction, in conjunction with the force which is

comprehended by the mechanoreceptor, was the inspiration behind building the second part of the tissue characterization system for MIRS application. In this research, in order to measure the tactile force between tissue and robot, the robot is equipped with a tactile force sensor which enables the robot to measure the contact force of the tissue interaction. The strain-gauge, consisting of a ball-caster, measures tactile forces with an accuracy of 0.01 N which are then transferred to the tissue characterization algorithm.

During contact between tissue and sensor (see Figure 3), the system starts to behave in a similar manner to that of a real surgeon's hand during an operation. When a surgeon palpates a tissue for examination, he/she first touches then indents the tissue and the resulting kinesthetic and tactile feedback message to the brain permits a determination to be made as to tissue softness and other material consistencies. The developed system, based on the human haptic system, operates in a similar manner to the surgeon's hand. Operated by the user, the tip of the sensor mounted on the robot touches the surface of the material. The force feedback control (FFC) then takes over control of the robot (Figure 4) and stabilizes the contact between the ball caster and tissue. Then, the robot starts to mimic human palpating behavior in order to scan the surface while the controller ensures that the robot neither indents the surface nor becomes separated from the tissue surface. The palpation field is defined by the desired center and radius which are chosen by the user. The robot touches the center and moves in a spiral movement which covers the desired field after which a 2D/3D profile of the touched tissue is shown to the user.

By knowing the topography of the tissue, the system is able to calculate the modulus of elasticity of the desired point on the tissue surface. The robot indents the ball caster on the desired point and develops a contact detection algorithm (CDA) in order to calculate the depth of the indentation after which the result is fed to another algorithm that calculates the modulus of elasticity of the goal tissue in real-time. Depending on the result, either 2D or 3D scanning is chosen in order to obtain the tissue profile and a related depth calculation algorithm is activated automatically to calculate the depth of the indentation.

Another feature of the developed system is its ability to map tissue abnormalities in terms of (relative) softness. The material characterization algorithm is capable of scanning the surface of a nonplanar material while the depth of indentation is kept constant. As a result, the algorithm calculates the relative softness of any abnormal tissue points which has a different softness in

comparison to adjacent points. The block diagram of the whole developed artificial system is shown in Figure 4. Each section will be discussed in detail.

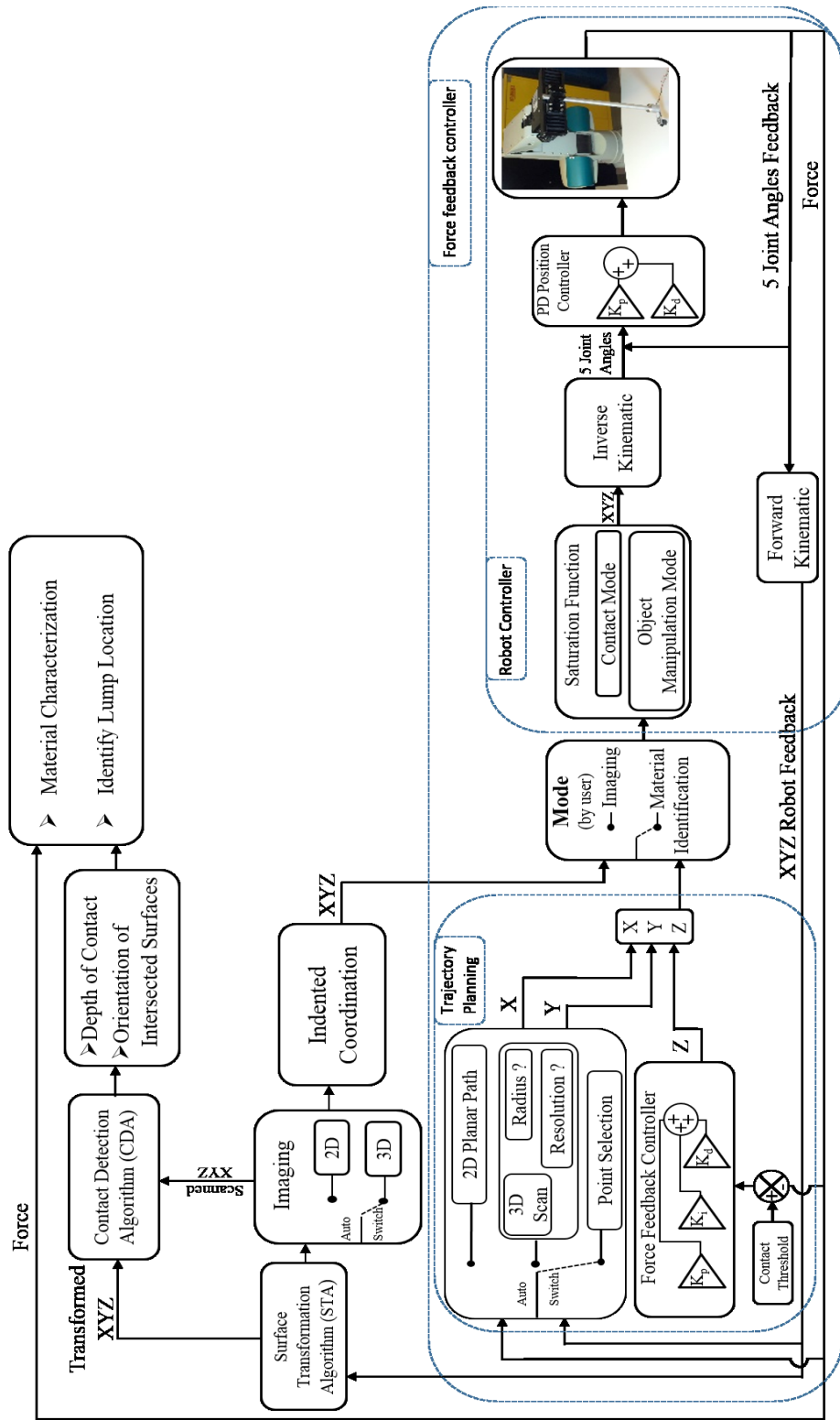


Figure 4. Material characterization system block diagram

2.2.1 Manipulator with force feedback

The manipulators used in RMIS consist of serial and parallel mechanisms. The articulated prismatic and revolute joints are designed to execute precise maneuvers which are issued by the master part of surgical tools. In current research, and since the focus is on the interactions that occur in the slave part of robotic tools, a simulation is designed in Matlab Simulink environment to operate as the master part. The virtual master part, which is the user interface of the system, receives user's input and transfers the desired operation followed by the slave part [47]. These operations consist of approaching and touching the surface of a material, palpating the tissues topography and indenting the desired point to calculate the modulus of elasticity.

The QUARC accelerate design package (version 2.3.603), which is product of Quanser inc. is integrated in Matlab/Simulink package 2012b (version 8.0.0783) is used to implement the force feedback control. Since the Quanser control works with a time iteration of 0.001 sec, and in order to have stabilized synced sub-systems, the other algorithms are programmed to work with the same time iteration. As a result, the algorithm's processes, which are computationally expensive, are assigned to be performed using three PCs connected to each other using Quanser stream call/write block over a local network which is specifically designed for mentioned tasks. In order to assure that the inherent delay in real-time operations does not adversely affect the system, a test is designed to measure any delay in the control loop. A delay is defined as being that period of time in which a transmitted signal travels through the two other PCs and returns to its point of origin. Such a delay test is implemented for each PC and the maximum delay of 0.0034 seconds, which is accumulated during 20 minutes of active working of the system, is introduced as the whole delay of system.

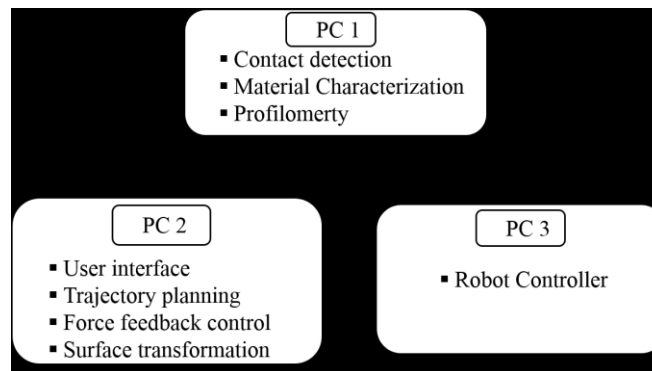


Figure 5. Distributing the real-time calculations on three PCs

2.2.1.1 Robot Position Control

The Catalyst-5 robot, which is used to execute as the master part, is controlled by the Quanser open architecture module [48]. The inverse kinematic approach [42] for object manipulating, and reaching the desired coordination of ball caster sensor in Cartesian space, is used in the module. The kinematics of the designed probe, which connects the gripper to the force sensor, is also added to the kinematics of the robot. Five proportional-derivative (PD) controls are used to control the angle of each revolute joint of the robot. The QUARC software, which is integrated in Matlab Simulink environment, is utilized to apply the PD closed-loop position controller for reaching the desired coordination of the ball caster as shown in Figure 4.

2.2.1.2 Controller with force feedback

Robots contact the environment for different purposes such as object manipulation [49], tactile servo-operations [50] and rolling manipulation [51]. In these procedures, equipping the robot with a tactile sensor can provide the information related to the contact such as detecting the contact itself, calculating contact area surface [52] and acquiring the force resulting from the intersecting surfaces in the contact field. Force feedback can also be used for robot control strategy. For example, Denie *et al.* proposed a control strategy of the robot based on a developed large scale tactile map of the robot. Their architecture represents different phases which should be considered for tactile-based control and representation [53]. Wang *et al.* designed a hybrid impedance control which enables a 5 DOF robot to follow both the positions and trajectories. The force and torque feedback, captured in the end-effector of robot, were used in the closed-loop control of the robot [54]. In current research, the force feedback is also used in controlling the robot to have stabilized contact between the sensor and goal tissue. The micro load cell (model No. 3132 and manufactured by Phidget Inc.) is used to transfer a continuous stream of force data into Matlab Simulink environment using a USB port [55]. The load cell is a force module which works by sensing microscopic changes on the beam element of the sensor. The manufacturer of the sensor, which has a capacity of 780 gr., indicated that the error is equal to 1% of the measuring range [56]. As shown in Figure 6, the strain gauge is attached to a probe which is designed to connect the sensor to the gripper of the robot. The other side of the force sensor is connected to a 0.5 in. ball caster manufactured by Pololu Inc. The ball caster enables the sensor to rotate on the surface of the material while the force sensor continuously measures

the contact force between the ball and the tissue. The strain gauge is calibrated to capture the force using the configuration shown in Figure 6.

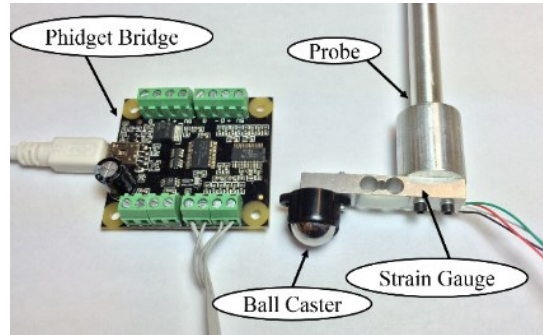


Figure 6. Force sensor element including ball caster, strain gauge and Phidget Bridge

By applying the position control strategy, the ball caster sensor can approach the zone that is specified by the master part. The area is, in fact, where the artificially made silicon rubber material is located. This area represents the surgical field during a simulated RMIS experiment. The silicon rubber plays biological tissue's role in validation step of the proposed system. Eq (1) shows the dynamics of the robot which interacts with external environment.

$$M_d \ddot{x} + B_d \dot{x} + K_d (x - x_d) = -F_e \quad \text{Eq (1)}$$

Where: x , \dot{x} and \ddot{x} are the corresponding position, velocity and acceleration of the touching ball caster, x_d the reference position of the ball caster, M_d , B_d , K_d are inertia, damping and stiffness of the system, and F_e is environmental reaction force which is measured by the ball caster.

To control the system, a force feedback control (FFC) is designed as an admittance control approach. A proportional integrator derivative (PID) controller, shown in Figure 7, is used to control the position according to the force feedback of the robot [57]. The controller is designed to stabilize the force to the threshold of 0.04 N which is defined as the touching force. When the robot approaches the surface of a material, and contact is made between the ball caster and material, the system automatically engages the force feedback controller (FFC) so therefore no separation or indentation occurs.



Figure 7. Admittance control approach

The stabilizing force varies according to the material softness and its nonlinear behavior. The FFC controls the vertical motion of the robot in such a way that the force which is produced because of sensor-tissue interaction doesn't exceed the predefined contact force. The stabilization force for two silicon rubber specimens, made by Ecoflex 00-10 and softened with silicone rubber oil, is shown in Figure 8. As can be seen from this graph, the stabilization time for harder a material with 32 KPa occurs in 0.15 Sec the duration for the softer one with 0.8 KPa is 0.38 Sec. The stabilization process for the softer Ecoflex 00-10 is accompanied by an indentation of 0.1 mm in the vertical direction which is recorded by the robot's positioning control feedback.

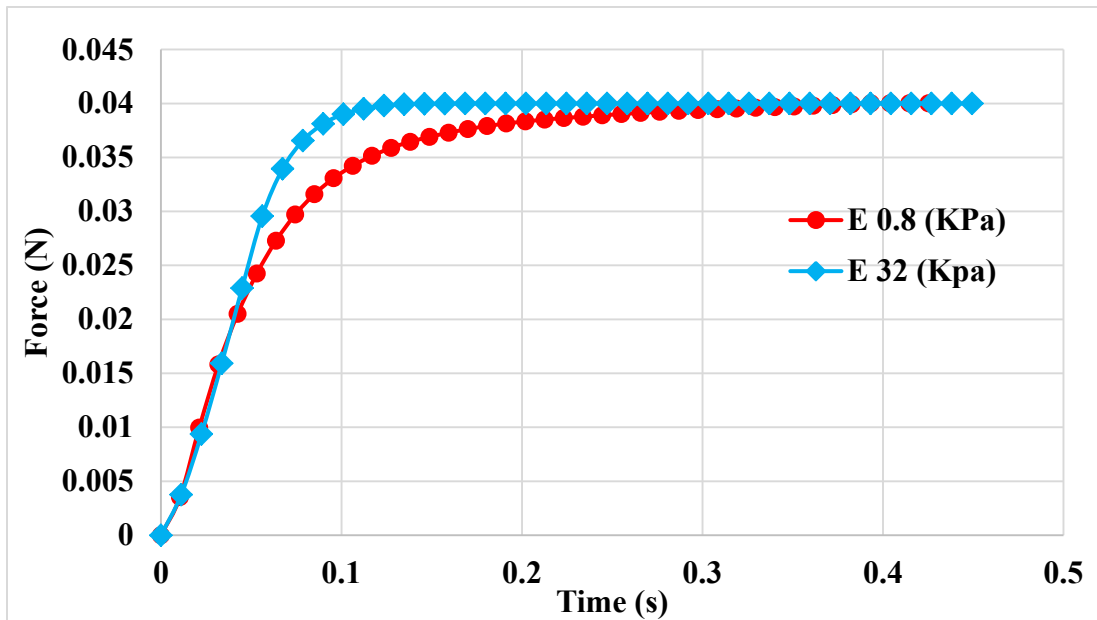


Figure 8. FFC stabling force on surface of material with 32 KPa and 0.8 KPa elasticity modulus

The FFC is designed to stabilize the contact for both the static and dynamic position of the robot. Figure 9 shows that if the straight motion is defined for the robot as a prescribed path, the ball caster will have spatial movement which is tangential to the surface of the tissue. During this

spatial motion, the FFC keeps the force to the touching threshold. Consequently, the ball rotates on the surface and saves the scanned contact point without indenting the material. While the ball scans the material surface, a surface transformation algorithm (STA) calculates the spatial position of the surface using the saved contact points. The procedure is discussed in section 2.2.2.1.

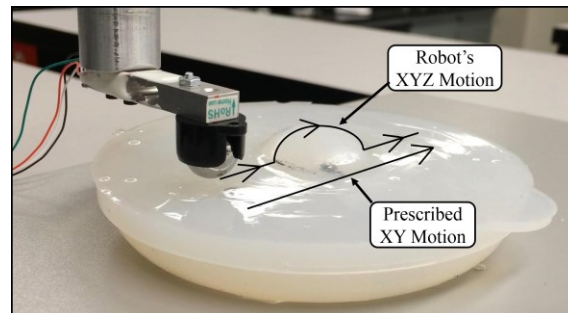


Figure 9. Robot 2D maneuver with FFC

The spatial position is a result of joint to Cartesian space conversion in forward kinematic algorithm of robot as shown in Figure 4. The velocity of the robot in each X, Y and Z direction is saturated by a rate saturation function for both modes of contact and object manipulation. The velocities are saturated to 50 mm/s in each direction for the object manipulation mode. As soon as contact is made, the rate saturation block limits the velocities to 5 mm/s for each direction. Consequently, the robot which has force feedback can move at a rate of 8.66 mm/s in the 3D workspace when it interacts with the external environment.

In order to evaluate the FFC control in 3D motion, a complex maneuver on the surface of very soft foam is defined. The selected foam, which is shown in Figure 10 (a) has a modulus of elasticity equal to only 0.2 KPa and can therefore easily be deformed. While the robot scans the surface, the FFC attempts to keep the force to 0.04 N. The steady state error, which is captured during the 100 mm prescribed path, is illustrated in Figure 10 (b). The reference force is defined as 0.04 N for the FFC during this maneuver. Different errors are measured for two phases of mounting, both uphill and downhill. The force deviation and errors are shown in Table 1. Verification of the captured surface, and the procedure in which the topography is calculated, is discussed in 2.2.2.1.

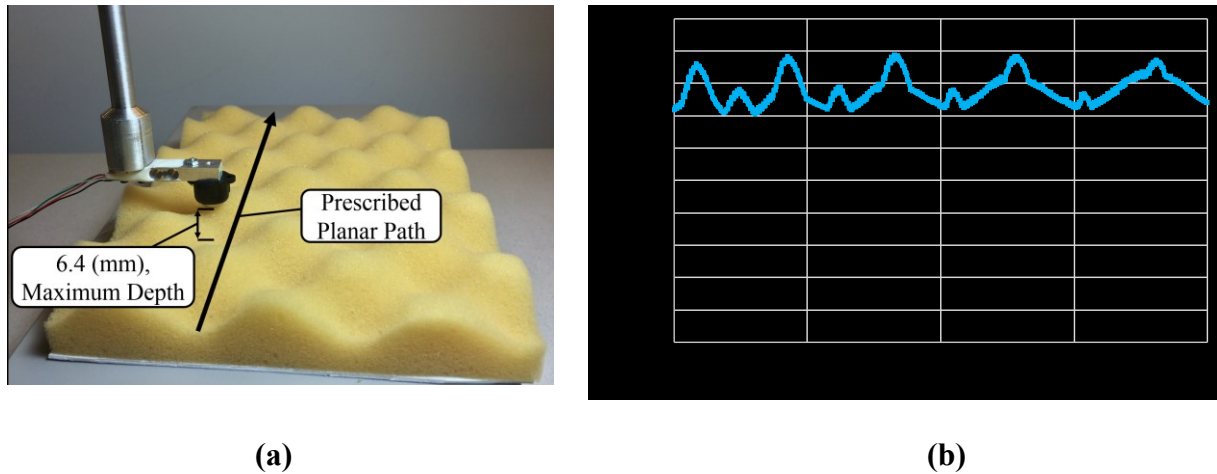


Figure 10. (a) Passing on bumpy surface (b) Steady state error of the FFC in force stabilization during the passed distance

Table 1. Steady state error of FFC for the touched length shown in Figure 6. (a)

Mode	Deviation Force from Reference Point (N)	Error (%)
Going Uphill Scanning	Max Captured Force : 0.0445	11.25
Going Downhill Scanning	Min Captured Force : 0.0351	12.1

2.2.2 Profilometry of organ with natural shape

The material characterization methods which are discussed in context of tactile sensors are interconnected with the two main topics of stress and strain [58]. Researchers have used different types of tactile sensors such as piezoresistive, optical, pneumatic in order to measure the force in the contact area for MIS and RMIS applications. However, applying the developed method for in vivo applications is still remained a challenging task. Most of the experiments to obtain mechanical properties of tissue were conducted on desired excised tissue specimens [30]. Ottensmeyer *et al.* quantified the different responses which are seen between excised lobe case and the in vivo whole organs. They reported that different testing conditions led to getting different properties of the tissues [35]. Different results of experiments, conducted on excised tissue and in vivo organs, were mainly due to: (i) the lack of perfusion in absence of the vessels [35], (ii) the dehydration effect [59] and (iii) the natural geometry of the organ. The developed

system in current research focused on an applicable method which can measure the organ's mechanical properties in the natural geometrical condition. As result, profilometry of natural shape organ will be the first step in tissue characterization procedure.

Most of human organs have unsymmetrical and nonplanar geometry. As a result, the tactile sensor which characterizes the contact for in vivo applications should deal with the non-uniform geometry of these tissues. The imaging algorithm, shown in Figure 4, is capable of measuring the spatial position of a desired point on organ's surface. The developed system for acquiring the mechanical properties of tissue provides the user with three options. First, if the user selects the "point selection" and guides the ball caster to the desired point, the sensor touches the point while the FFC keeps the force to the threshold of touch and the surface transformation algorithm (TSA) saves the selected points coordination. Second, if the user selects the 2D option, the ball caster scans the path on the surface of the material between the two points which are defined by the user as shown in Figure 9. Third, if the user selects the 3D mode, the system scans the simulated surgical field according to the radius and resolution which are defined by the user. This information is fed to the artificial palpating algorithm which then calculates the tissue's softness.

The artificial palpating algorithm, which is involved in the 3D mode, is inspired from human's palpating behavior. One tries to touch and palpate a material without indenting to obtain the surface properties of a deformable material. Then, using a finger, the user tries to indent the surface precisely to acquire the softness through the human haptic feedback system and it is upon the basis of this procedure that the algorithm is designed to work. First, the FFC stabilizes the force on the defined center. Then, the robot sweeps the ball on surface of tissue in a circular pattern-based path similar to the trajectory of a human finger. This non-straight trajectory is used also in medical diagnostics for lump detection [60].

The Archimedean spiral equation is used in the 3D scanning mode to recreate human palpating behavior. The X and Z coordination of 3D scanning algorithm are calculated using Eq (2). The Z coordination is obtained by FFC and sent to the robot.

$$X = X_0 + r.Cos(a.r) \quad \text{Eq (2)}$$

$$Y = Y_0 + r.Sin(a.r)$$

(X_0, Y_0) is the center coordination of the area around which scanning takes place. r is the radius of the area for spiral scanning and a is the resolution factor of the scanning and is defined by the user through the interface. The trajectory points are calculated proportional to the scanning resolution factor. Two series of calculated trajectories with different resolutions are shown in Figure 11. The X and Y coordinates are the outputs of the 3D trajectory planning algorithm. The Z coordinate is the output from the FFC which is integrated in the trajectory planning. These three outputs are set as the reference of position control which are to be followed by the robot. By knowing the relative coordination of the touch point, the 3D profile of the scanned tissue can be achieved. The forward kinematic approach is used to calculate the relative Cartesian location of touched points. The feedback of the robot, which is the measured angle of each joint, constitutes the joint space of the robot. The joint space to Cartesian space transformation is undertaken in the forward kinematic block shown in Figure 4. The result of this transformation is the Cartesian coordination of the ball center and the resulting information is used in STA to calculate the exact touched point locations with respect to the saved ball center coordination.

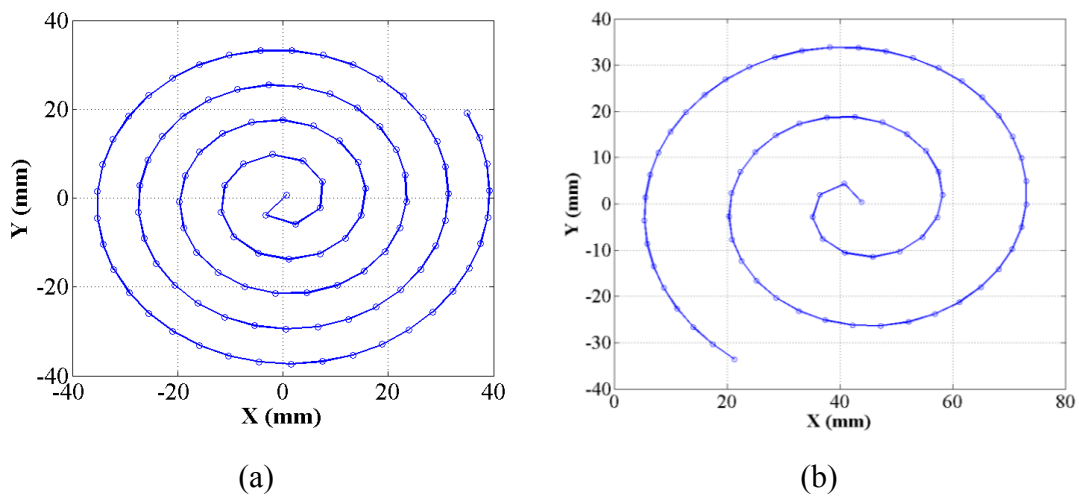


Figure 11. Produced X and Y trajectory to be followed by the robot, (a) Radius: 20mm, distance between nodes: 5.5mm (b) Radius: 20mm, distance between nodes: 5.5mm

2.2.2.1 Geometry correction of scanned surface

Surface metrology science, which studies surface properties in small scale geometrical features, has been used in different engineering disciplines such as machine tools [61], vehicle dynamics [62] and biological applications [46, 63, 64]. In order to acquire precise surface information, as a result of a rolling tribological ball contacting the surface of a tissue [65], appropriate transformation calculation should be done. In current research, the true surface profile of the tissue is obtained using the ball center locus. As shown in Figure 12, as the ball rotates above the surface the forward kinematic feedback of robot saves the coordination of the ball center. This point is representative of the real corresponding contact point from which the real surface coordination is calculated based on the scanned surface. The same transformation is also necessary to obtain the true surface in context of the rolling ball in other applications. For example, the true envelope surface should be calculated based on the morphological filter which reflects the boundary surface region in measuring roughness using a rolling ball [66]. Also, in tire-road interaction the ground profile can be calculated using the instantaneous center (IC) of the tire [67] when it filters the small frequencies of the road.

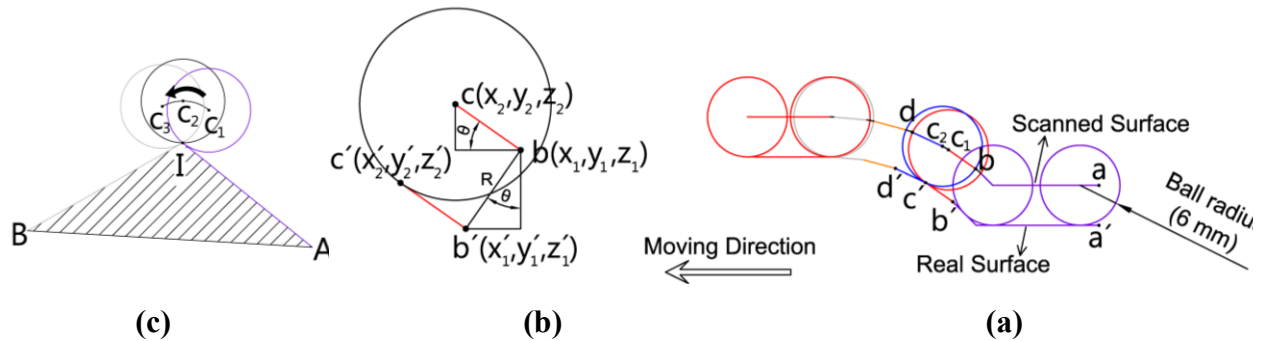


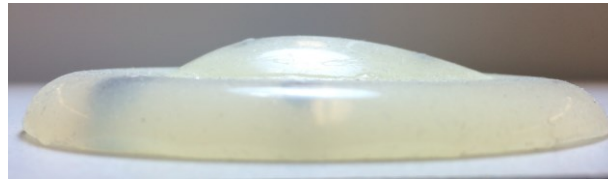
Figure 12. (a) Scanned and real surface of the tissue, each segmented color represents the real corresponding surface of the same color (b) Translational movement on $b'c'$ which is saved as $bc1$ (c) Passing the ball center on a sharp edge, the blue circle is tangent to the AI and the gray circle is tangent to IB . Point I is the center of $\widehat{C_1C_2C_3}$

As can be seen in Figure 12 (a), the real surface of the tissue is shown in several segments. Each segment represents the corresponding scanned surface which is shown with the same color. The

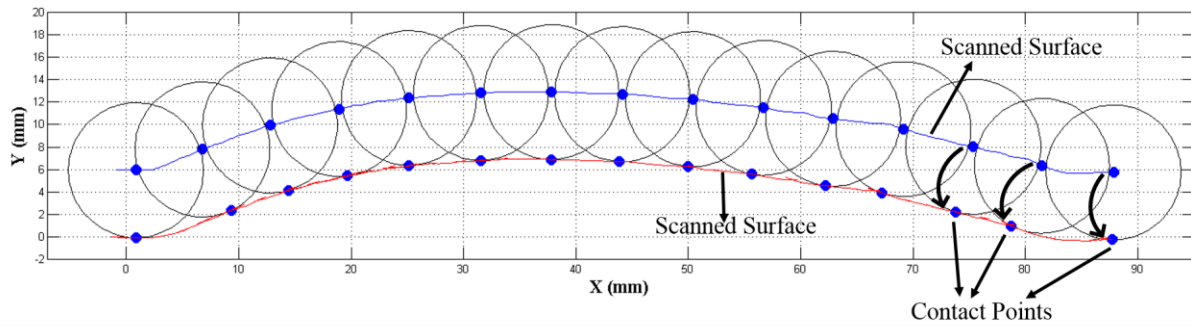
scanning accuracy depends on size of segment which the system is able to detect. The Scanning resolution is equal to the Cartesian resolution of the robot which is 0.1 mm. It can be seen that the segment of bc_1 is saved as $b'c'_1$ on the real surface in Figure 12(b). The transformation matrix which locates the point b' is defined by Eq (3). Location of each point is calculated based on the slope of the line which will the ball will contact in next step.

$$\begin{bmatrix} x'_1 \\ y'_1 \end{bmatrix} = \begin{bmatrix} x_1 - R \cdot \sin(\theta) \\ y_1 - R \cdot \cos(\theta) \end{bmatrix}, \theta_1 = \tan^{-1}\left(\frac{y_2 - y_1}{x_2 - x_1}\right) \quad \text{Eq (3)}$$

The STA transforms the point b to b' , when the ball center reaches to point c . The real surface of the scanned tissue is formed by many linear segments. The STA constructs each point of the straight segments with one-step delay. The result of the TSA transformation for the elliptical shape surface is shown in Figure 13. In this figure, only several ball contact points from thousands are shown and constructed the red scanned surface.



(a)



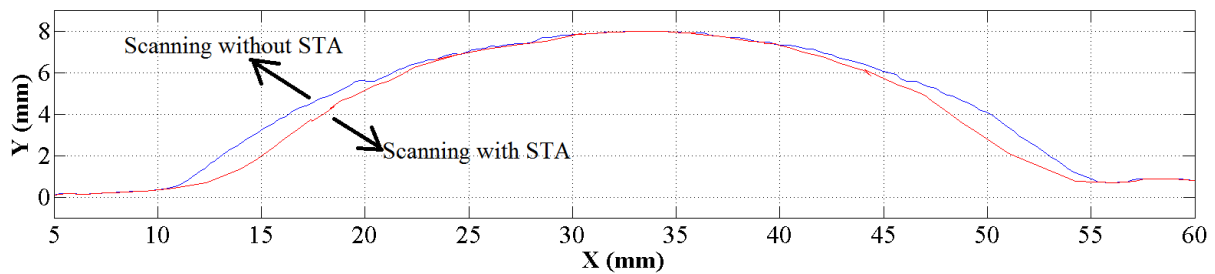
(b)

Figure 13. (a) Elliptical shape built by silicon rubber material Ecoflex 00-10 ($E= 0.8$ KPa) (b) 2D STA transformation for specimen shown in (a). Each blue circle on scanned surface is transformed by TSA from the scanned surface

The specimen shown in Figure 13 is built with an elliptical molded shape, which is similar to the organ's natural shape. The STA correction importance is more critical when it deals with a smaller surface radius in comparison to that shown in Figure 13. To compare the STA operation, a specimen with a higher convex contour is prepared from the Ecoflex 00-10 material. This specimen has the maximum convexity which the system can be used for scanning. The maximum angle that a 6 mm radius ball can implement scanning is 30° and if this angle is exceeded, the ball container part of the sensor will contact the specimen and hence the frictionless contact assumption between tissue and ball will not be valid.



(a)



(b)

Figure 14. (a) Spherical shape specimen which is made of Ecoflex 00-10 0.8 KPa

(b) Scanned surface with and without STA

A similar transformation, as discussed in the 2D movement, is used for 3D scanning for which the explicit transformation shown in Eq (4) is used to acquire the ball contact points.

$$\begin{bmatrix} X'_t \\ Y'_t \\ Z'_t \end{bmatrix} = \begin{bmatrix} X_t - R.\text{Sin}(\theta_{xy}) \\ Y_t - R.\text{Cos}(\theta_{yz}) \\ Z'_t - R.\text{Cos}(\theta_{xz}) \end{bmatrix}$$

Eq (4)

$$\theta_{xy} = \tan^{-1}\left(\frac{Y_{t+1} - Y_t}{X_{t+1} - X_t}\right), \theta_{yz} = \tan^{-1}\left(\frac{Z_{t+1} - Z_t}{Y_{t+1} - Y_t}\right), \theta_{xz} = \tan^{-1}\left(\frac{Z_{t+1} - Z_t}{X_{t+1} - X_t}\right)$$

Each spatial change in location of the ball center is imaged on three planes, XY, YZ and XZ. The TSA then calculates the angle of each planar change in these 2D coordinates. All mathematical transformations occur in each integration of the Matlab/Simulink by the STA block. The result is shown in Figure 15.

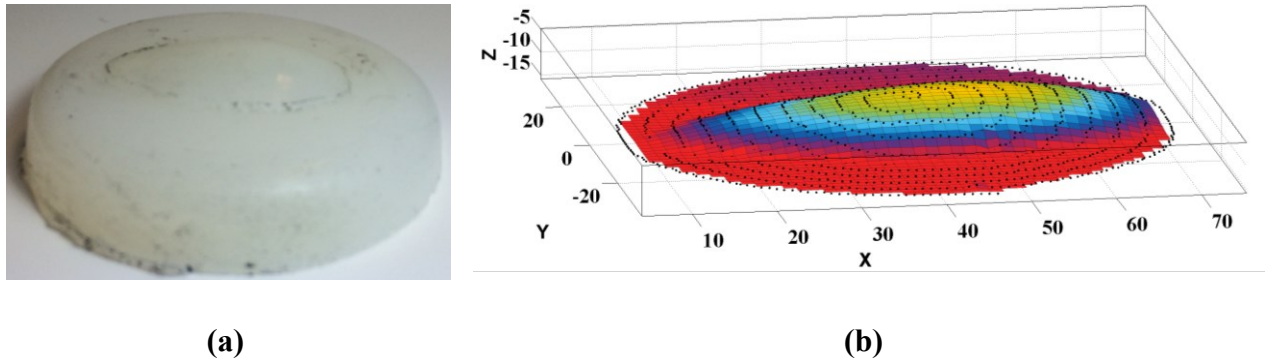


Figure 15. (a) Built elliptical silicon rubber (Ecoflex 00-10 base softened with silicon oil) (b) Scanned elliptical material with ball caster

Human organs such as the liver and kidney have smooth surface shapes. Although the tissue profile similar to the surface which is in Figure 12 (c) is not the same as a human organ surface profile, the proposed method of acquiring the tissue surface profile with a rolling ball is developed to scan even this kind of jagged surface. As shown in Figure 12 (c), the rolling ball in the AIB direction rotates on the AI path until it reaches point I which is the instantaneous center of the ball in motion. Then, the ball center rotates around point I until the circle becomes tangential to path IB. In this step, the transformations which are presented in Eq (4) and Eq (5) do not reflect the points of the real surface of I. An algorithm which detects the rotation around a jagged point has also been developed and added in the STA. By knowing the rotation around a

certain point, point I which is the real point of the surface should be the output of transformation for the C1C2C3 arc. In order to detect if the ball center has pure rotation around a certain point, the radius and center of each three sequential points are recorded every 3 mm. For each ball center point, which is the output of forward kinematic, the TSA selects the two next points at a distance of 3 mm. The coordination of these three points are fed to the circlefit3d toolbox in Matlab [68]. If the calculated radius for these three points be located in range of the ball radius with 15% tolerance (5.1 mm to 6.9 mm), and center of fitted circle on the three points be in neighborhood of 2 mm distance of previous step points, then these three point will be part of the a circle. As a result, point I will be transformed by STA as the arc C1C2C3. The 15% tolerance is achieved practically for the sharp edge for which the AIB angle is between 110° to 160° . This tolerance should be considered because of the geometrical and computational errors which have different impacts on the circle fitting procedure [69, 70]. During the tissue scanning procedure in current research the curve radius calculation algorithm was active, but there were no jaggy points detected by the algorithm. This part is added to present a comprehensive method of scanning the surface using the rolling ball.

2.2.2.2 Profilometry validation

In order to validate the imaging module, which is part of developed tissue characterization system, an evaluation procedure is defined. Several silicon rubber specimens are built using elliptical shape molds as shown in Figure 13 (a) and Figure 14 (a). The cured material is part of an elliptical surface which represents the goal tissue. Then Ecoflex 00-10 as base material and silicon oil were mixed. Adding more silicon oil decreases the softness of the cured material. The constructive composition ratio of the materials is considered in such a way that the modulus of elasticity for cured material results in elasticity modulus of 0.8 KPa, which is softer than the selected real tissues in the experiment. The elliptical surface shape, shown in Figure 15(a), is selected for the validation test.

In order to obtain an accurate 3D shape of the molded material, an LPX-250 Roland PICZA 3D laser scanner is used to scan the specimens with accuracy of 0.3 mm in the X, Y and Z directions. The points of scanned cloud are obtained in the coordination matrix using Dr. PICZA software [71]. The coordination, which is acquired using 3D scanner, is considered being the

error-free reference as shown in Figure 16(a). The output of the imaging block, which is a result of the STA, is then compared to the laser scanner surface output.

An iterative closest point (ICP) algorithm [72] is used to compare the point clouds which are saved from the robot and 3D scanner. The ICP toolbox by Kjer and Wilm in Matlab is used to compare the clouds [73]. The method works based on minimizing the root mean square (RMS) error during the registration of the two surfaces on each other. The ICP algorithm calculates the transformation and rotation matrix to register the two surfaces which are shown in Figure 16(a). As shown in Figure 16(b), the ICP algorithm registered the ball scanned surface on reference one. Calculated root mean square, in each iteration during brute force matching, reveals a 4.22 % error of the mechanical ball scanning method as shown in Figure 16(c). The result indicated that the scanned surface, using our proposed method, can be a reliable base for the depth calculation during material characterization processes.

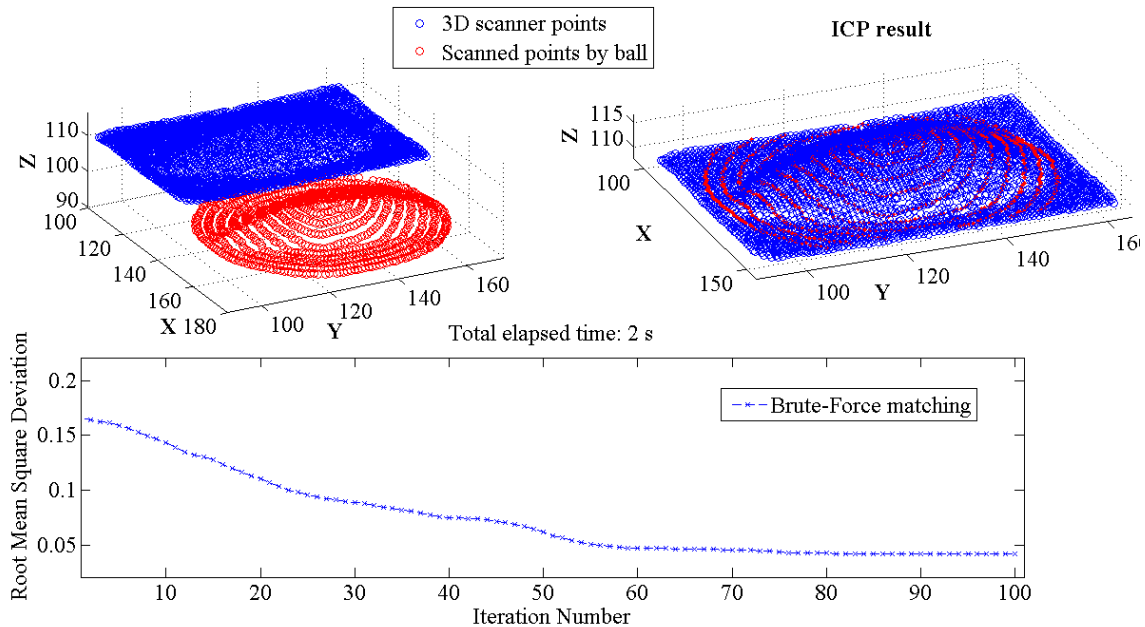


Figure 16. (a) Scanned surfaces with rolling ball and 3D scanner (b) Iterative closest point algorithm result, the scanned cloud by the 3D scanner is considered as reference (c) Root Mean Square error which is calculated for each iteration

2.2.3 Tissue characterization system and surface profile display

By knowing the accurate surface profile of the tissue, together with the known position of the ball caster which interacts with tissue, the contact between the material and tissue can be characterized. As a result, when the user selects the desired point for material characterization, different sub-algorithms will be engaged automatically. These algorithms are contact detection, depth calculation, the estimation of plane orientation for intersected plane and the characterization of the indented material.

2.2.3.1 Contact detection and contact depth

The indentation depth can be calculated by the characterization of the contact. To achieve this goal, two different 2D and 3D contact detection algorithms are designed. Each module characterizes the contact according to the mode selected by the user. The contact detection approach in current research works according to geometrical analysis.

2.2.3.1.1 2D contact detection

For the 2D mode, the CDA examines the coordination of the 2D scanned surface which are located in a range defined by a half-circular space. The center of this space is the ball caster coordination. The radius of half-circle is set to 8 mm to cover the 6 mm ball indenter. In each iteration of the controller, 0.001 seconds, two detected contact points which are representative of the contact boundary are detected as shown in Figure 17(a) and (b). The depth of the indented ball is calculated with respect to these two contact points. As the user guides the sensor toward the desired point in surgical field, the center of the ball is continuously located by the forward kinematics of the robot. The outer boundary of the ball is tracked with the circle range searcher sub-algorithm, which is included in the contact detection module. The half-circle space is defined by the circle equation and the center point. The algorithm detects the points of the material surface if the distance between the ball and surface is less than 0.1 mm. The locations of these detected points are fed to a depth calculation block. Two points which have maximum distance between detected points are selected as being the contact boundary. As a result, points C_1 and C_2 are continuously located during material indentation as the boundary points of the contact as shown in Figure 17.

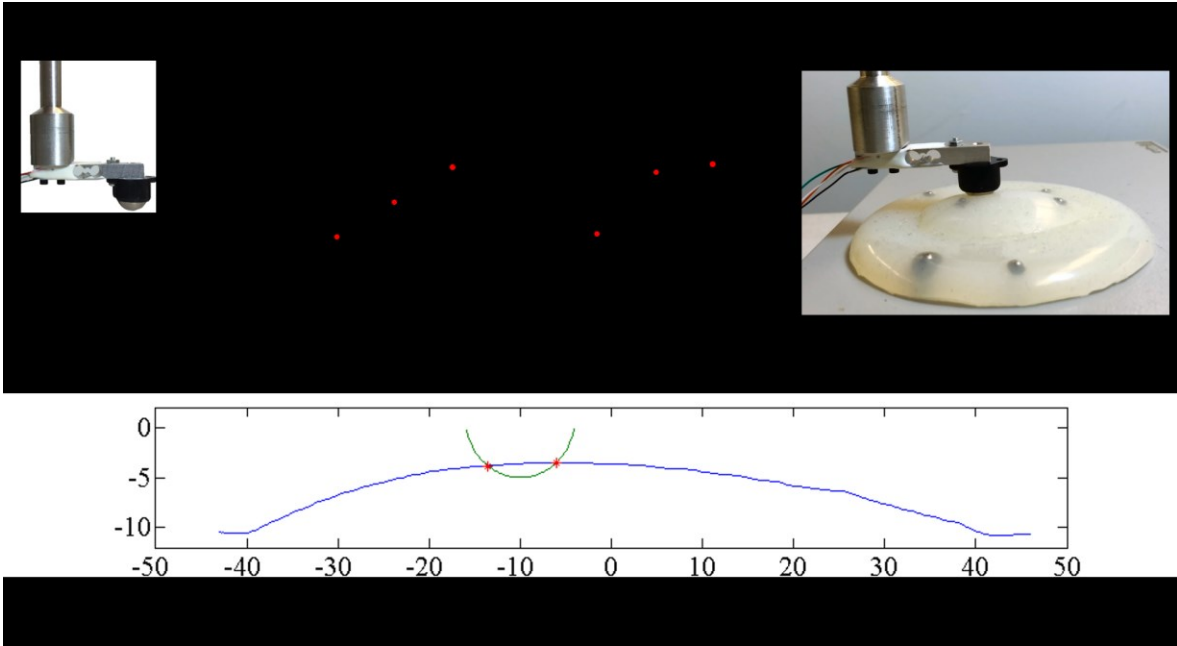


Figure 17. (a) Indented spherical ball on a tissue with curvature surface (b) Contact boundary points of the indented ball and nonplanar tissue (c) Enlarged contact area (d) Indented ball on surface of Ecoflex 00-10 (e) Detected points of contact for the moment which is shown in (d)

By knowing the contact point's positions, the depth of contact can be calculated through geometrical calculation. The contact depth of the ball caster consist of two lengths, i_1 and i_2 , as shown in Figure 17(a). i_1 can be calculated using Eq (5), the relation between the intersected cords of a circle.

$$i_1(D - i_1) = \left(\frac{AB}{2}\right)^2, \quad i_1 = \frac{D - \sqrt{D^2 - C_1 C_2^2}}{2} \quad \text{Eq (5)}$$

The similar neighborhood search method, which is applied for contact point detection, is used to calculate i_2 . Another range searcher [74] sub-algorithm in CDA calculates the minimum length among point C and the saved surface profile points. The maximum length of i_2 is 1.2 mm and is experimentally measured for a 6 mm radius ball on the surface of a material having a minimum curvature of 40 mm. The range searcher algorithm searches the contact point in a range of 1.2 mm to find a point which has minimum distance to point C [75]. The range can be modified for the other size of ball. The resulting i will be used to calculate the modulus of elasticity in the material characterization process.

2.2.3.1.2 3D contact detection

The 3D contact detection algorithm detects the spatial coordination of the boundary contact points between the indented ball and the scanned surface. The detected points shown in Figure 19(a) are obtained by fitting a surface on a circular boundary points. When the ball is indented on the surface, the real detected contact boundary may be located on the spiral line shown in the Figure 15(b). Consequently, the contact cannot be detected on this discrete surface. An interpolation should be done in 3D space to obtain indiscrete surface. The interpolated surface is a based locus for contact detection in 3D mode. The result of interpolation for Figure 15 (b) can be seen in Figure 19(b).

When a spherical ball is indented on the surface of material, the common points of contact which belong to both ball and scanned surface with a 0.1mm neighborhood are detected as contact points. These common points are shown on the surface in Figure 19(b) and (c). The indenter cloud is shown in Figure 19(c). The shape of this surface varies depending on the location of indentation. Since the indented ball is a rigid sphere and no deformation is considered for it, the normal of fitted surface on the detected points represents the normal interaction of the indented material. This normal vector will be used in force measurement during material characterization.

The fitted circle on the detected contact points is shown in Figure 19(a). As shown in Figure 19(d), for each state of movement a circle is fitted to the detected contact points. The diameter of the circle is calculated continuously during the indentation and transferred to the block which calculates depth of the contact. The diameter of the fitted circle is substituted with $C_1 C_2$ in Eq (5)

to calculate i_1 , and i_2 is calculated with a range searcher algorithm to find the minimum distance between point C' and the interpolated surface. The total i will be used for elasticity modulus calculation.

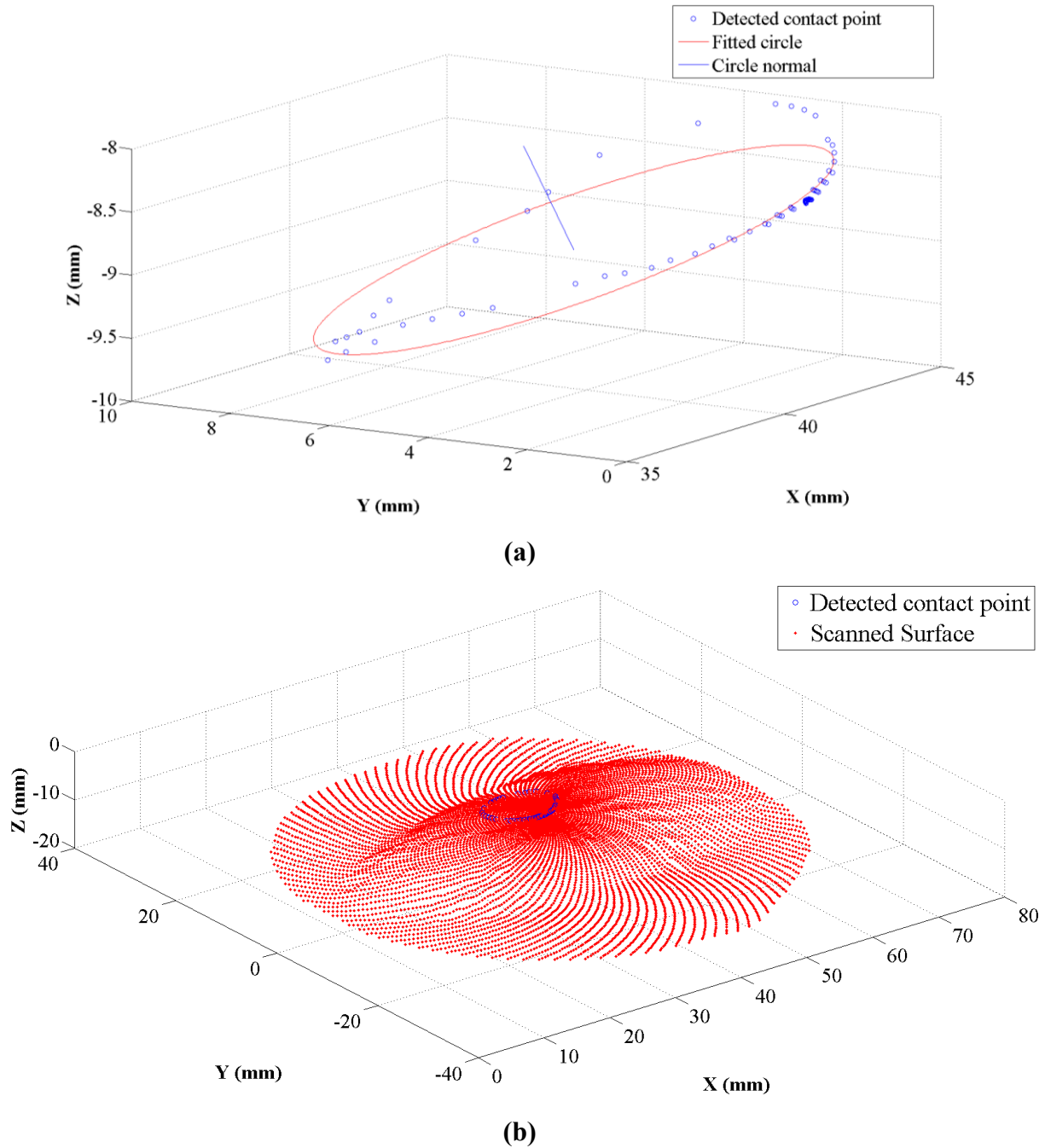
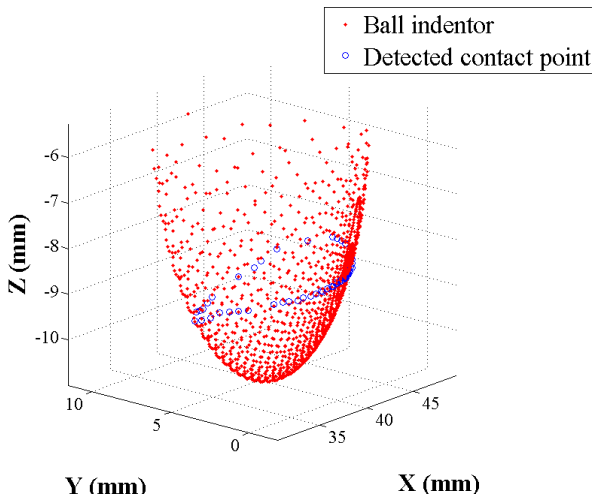
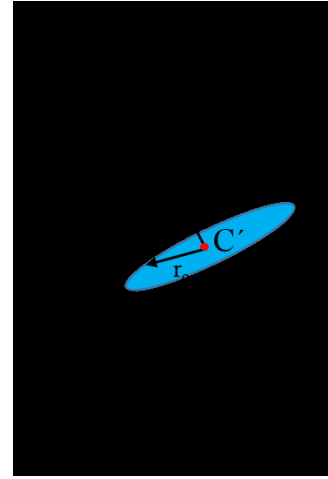


Figure 18. (a) Detected contact points on surface (b) Fitted circle on detected contact points (c) Detected contact point on lower hemisphere of ball which is indented on surface of material (d) Imaginary circular surface in contact area



(c)



(d)

Figure 19. (a) Detected contact points on surface (b) Fitted circle on detected contact points (c) Detected contact point on lower hemisphere of ball which is indented on surface of material (d) Imaginary circular surface in contact area

2.2.4 Tissue stiffness calculation based on characterized contact

Material characterization in current research is done by relating displacement and material surface and measuring the reaction force of the material [58]. The characterization can be implemented by calculating the depth of indentation and the normal interaction force of the tissue based on elasticity formulation. As shown in Figure 17, when the indentation increases the contact area and the volume of material which directly contributes in contact area changes nonlinearly. In current research, the maximum depth of indentation which is applied on material by a 6 mm radius ball is 3.2 mm. For this range, the linear Hertzian contact theory can be applied to calculate the modulus of elasticity [76]. Liu *et al.* validated the linear assumption by testing on various soft tissues [46]. They investigated as long as the indentation depth is kept small (<3.5 mm), the linear assumption in elasticity calculation for small deformation complies with other literature [31, 77, 78]. The general solution for contacting two spheres with an indentation of i can be calculated according to Eq (6) [79] as shown in Figure 20.



Figure 20. (a) Spherical indenter on spherical surface (b) Inclined indentation on material surface, F_s is measured by stain gauge and the n is the normal interaction of surface

$$i^3 = \frac{3}{4} \left(\frac{1 - \nu_{in}^2}{E_{in}} + \frac{1 - \nu_t^2}{E_t} \right) \frac{F^2}{R} \quad \text{Eq (6)}$$

Where ν and E are Poisson's ratio and modulus of elasticity, F is the force acting on indenter and "in" and "t" refers to indenter and tissue respectively. R is the effective radius of the two contacted surfaces.

$$\frac{1}{R} = \frac{1}{R_{in}} + \frac{1}{R_t} \quad \text{Eq (7)}$$

R_{in} is the radius of indenter and the R_t is radius of the circle on fitted scanned surface in 2D mode, or the radius of sphere which is fitted in 3D mode. Wanninayak *et al.* developed a ball indenter to measure indentation depth for nonplanar tissue profile, but their method only considered the angle between inclined surface and the direction of measured force and the radius of touched object which contributes in contact was not considered [80].

In Eq (6) by assuming that the steel rigid indenter impinges the tissue, the modulus of elasticity the tissue is derived by Eq (8).

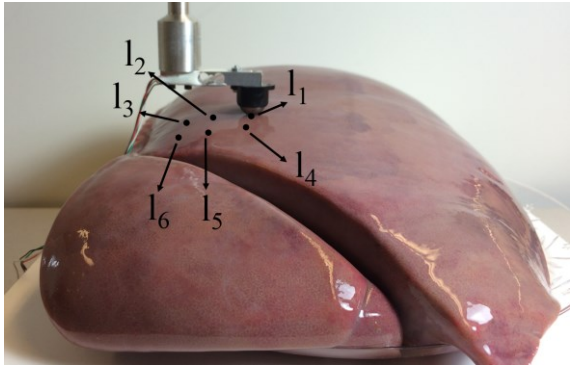
$$E = \frac{3(1-\nu_t^2)F_n^2 R_1 R_2}{4(R_1+R_2)i^3} \quad \text{Eq (8)}$$

As shown in Figure 20(b), the ball caster force sensor measures normal F_s , the force which is caused by the indentation in the vertical direction. Considering the homogeneity and isotropy of the linear range which is considered for Hertz contact theory, F_n can be calculated in the direction of normal surface interaction. The direction is normal to C_1C_2 in the 2D mode as shown in Figure 17(a). In the 3D mode, the direction is that of a normal circle which is fitted on a contact point as shown in Figure 20 (b).

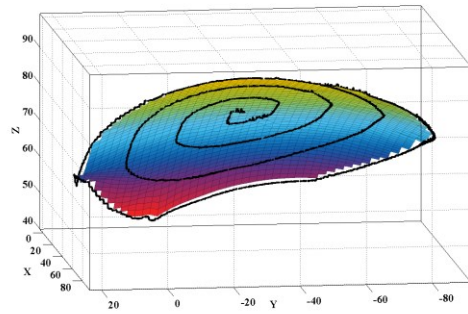
2.3 Result, discussion and performance analysis

The real-time material characterization which is presented in current research is tested on several biological tissues. The selected tissues are bovine liver, kidney and artery tissues. Brown *et al.* reported that the elastic response of soft tissue remains almost the same within three hours post-mortem [81] and the specimens which are used for experiments in the current project are implemented within that three-hour time span. The material characterization which is the major goal of the developed system is tested in 2D and 3D point selection modes. The result from each mode is compared with the two other modes, and the 3D mode results are compared to that found in other literatures.

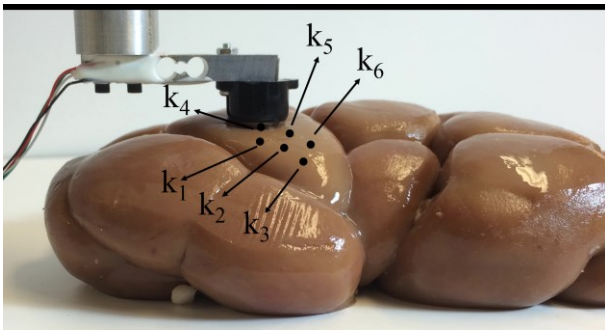
On each tissue, two series of points with three points in each series are selected to be identified by each material characterization mode. Since the data collecting procedure coincides with indenting the material surface, the specimens may lose the interstitial water which has hardening effect on tissues [59]. Therefore, testing a point more than two times is avoided. Point 1, 2 and 3 are selected for spot selection and 2D modes. And point 4, 5 and 6 are selected for 3D mode as it is illustrated in Figure 21 (a), (c) and (e). In order to compare the results of the three modes, it is endeavored that the selected points for 3D experiments be on the similar curvature of each tissue in order to obtain the same response from the tissues.



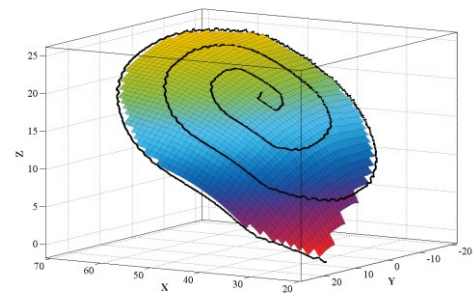
(a)



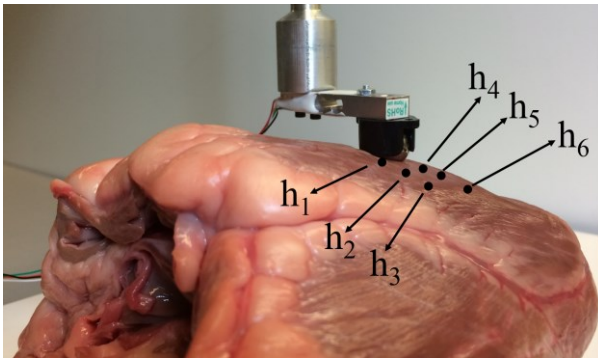
(b)



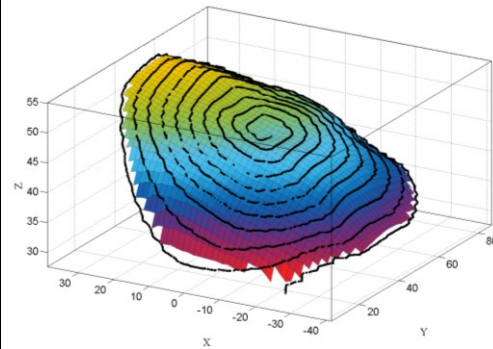
(c)



(d)



(e)



(f)

Figure 21. (a) Bovine liver (b) 3D scanned surface profile of the liver (c) Bovine kidney (d) 3D scanned surface profile of kidney (e) Bovine heart (f) 3D scanned surface profile of the heart

In point selection mode, the contact force between ball and tissue is stabilized by the FFC. Location of the contact point is saved as the reference level of measurements. After force stabilization, the prescribed vertical indentation of 3 mm is applied on the material surface. The modulus of elasticity is calculated for each point using Eq (8). In this step the material surface is assumed to be flat and the effective radius resulted by Eq (7) is equal to the indenter radius. The Poisson ratio of soft tissues which are considered as incompressible materials are in range of $0.45 < \nu < 0.49$ [77]. The Poisson ratio is assumed 0.49 for all of the specimens. The calculated E for each point calculated by spot selection mode is shown in Table 2.

Table 2. Elasticity modulus calculated in spot selection mode

Material	Point	Applied indentation (mm)	Calculated F_n (N)	E (KPa)
Liver	l_1	3	0.11	1.5
	l_2		0.09	1.0
	l_3		0.05	0.3
Kidney	k_1	3	0.31	12.2
	k_2		0.26	8.6
	k_3		0.22	6.1
Atrial	h_1	3	0.59	44.1
	h_2		0.46	28.0
	h_3		0.28	9.9

From the above table, it can be seen that there is a significant change between calculated E for point 1, which is on the flat surface of each tissue and point 3 where the surface has maximum curvature. As illustrated in Figure 17(c), when the vertical indentation of i_v is applied on the material surface, the effective indentation of i_e directly affects the normal interaction of F_n . As a result, the spot characterization will be accurate only for a flat surface.

The similar points which are used in spot mode are evaluated for material characterization in 2D mode. The straight path, which contains points 1, 2 and 3, is specified for 2D material characterization. The 2D profiles which are acquired by the STA are shown in Figure 22. The indentation and force calculations are undertaken according to these basic surfaces. When the ball scans the material surface, the contact point locations are calculated and saved by the STA. CDA calculates the depth of contact during indenting procedure. The result of 2D material characterization is shown in Table 3.

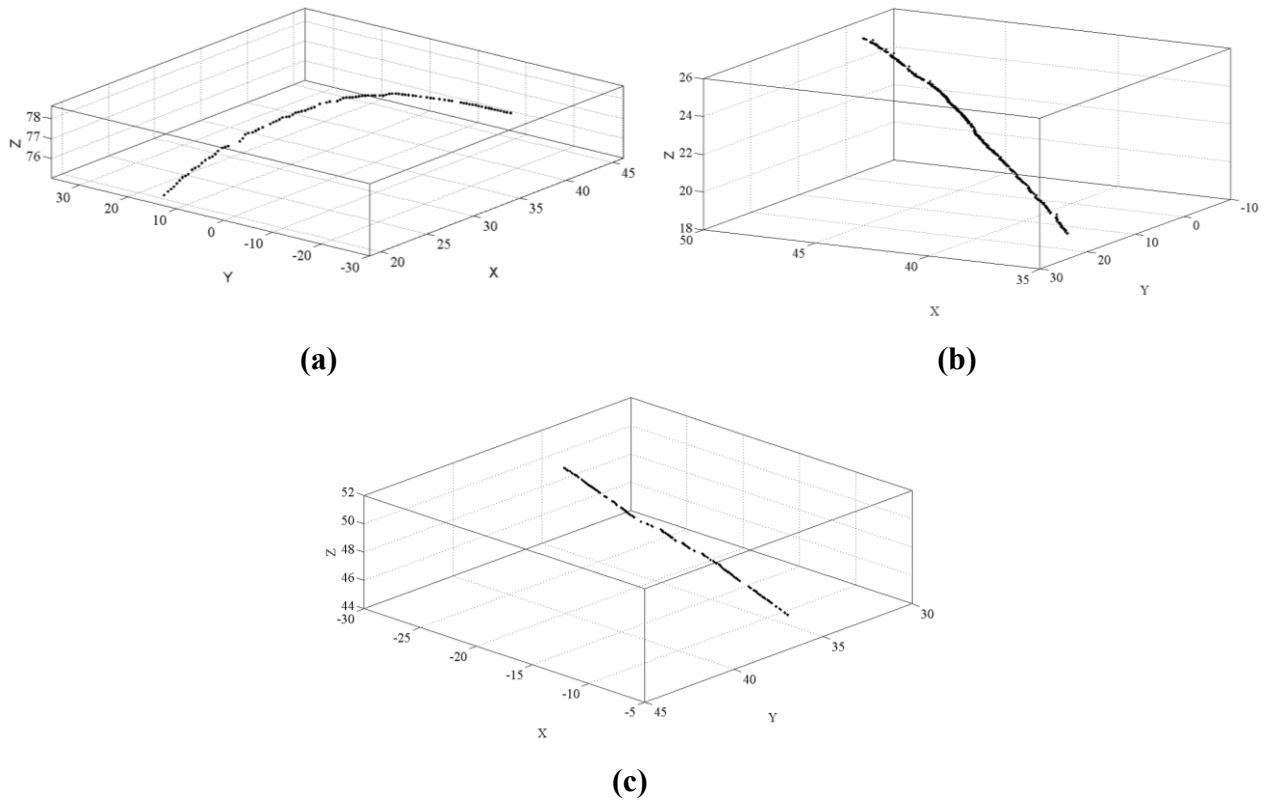


Figure 22. 2D Scanned surface profile of (a) Liver (b) Kidney (c) Heart

Table 3. Material characterization in 2D mode

Material	Point	R_{in} (mm)	Calculated R_t (mm)	Calculated i (mm)	Calculated F_n (mm)	E (KPa)
Liver	l ₁	6	155.2	2.80	0.11	1.8
	l ₂			2.77	0.09	1.3
	l ₃			2.30	0.06	1.0
Kidney	k ₁	6	50.9	2.96	0.31	11.3
	k ₂			2.83	0.28	10.6
	k ₃			2.70	0.26	10.5
Atrial	h ₁	6	57.6	2.95	0.61	44.9
	h ₂			2.54	0.47	41.7
	h ₃			2.29	0.34	29.8

The radius of the material surface is estimated in 2D mode and is taken into account in the elasticity calculation in Eq (7). The CDA also characterizes the contact geometry more accurately in comparison to the point selection mode so, consequently, the indentation depth can be calculated precisely. As shown in Table 4 the measured indentations are decreased by 23% for point l₃ and h₃, and 10% for point k₃ relative to calculated values in the spot selection mode. The measured contact force in normal direction (F_n) is increased by 20% for l₃, 18% for k₃, and 21% for h₃. Therefore, the calculated E has significant increase of 0.6 KPa (+60%) for liver at point l₃, 0.72 KPa (11.8%) for kidney at point K₃, and 19.9 KPa (201%) for heart tissue at point h₃. The result shows that the 2D mode efficiently characterizes the contact area in comparison to spot selection on curved surfaces.

Table 4. Comparison of Spot selection, 2D and 3D material characterization

	Point selection vs. 2D			2D vs. 3D		
	l_3	k_3	h_3	l_3 & l_6	k_3 & k_6	h_3 & h_6
Measured Indentation	-23%	-10%	-23%	-13.9%	-3.7%	+4.5%
Measured F_n	+20%	+18%	+21%	No change	+3.8%	+20.5%
Calculated E	+0.6 (KPa) (+60%)	+0.72 (KPa) (+11.8%)	+19.9 (KPa) (+201%)	+0.5(KPa) (+50%)	+0.7(KPa) (+6.7%)	+11(KPa) (+36.9%)

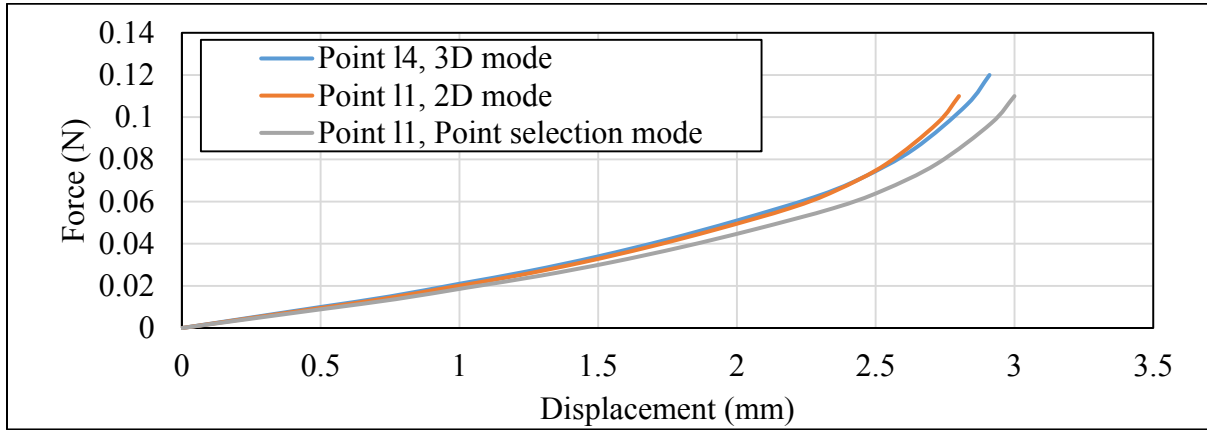
The second series of points, which are shown in Figure 21, are evaluated by 3D mode characterization. After specifying the radius and resolution of the desired area by the user, the STA calculates the 3D surface profile of the scanned area. In this mode, the user can guide the ball caster on each desired point in the scanned surface and then the selected point on the surface will be indented by 3 mm. F_n is captured for points 4, 5 and 6 on each specimen and the calculated E are shown in Table 5.

Table 5. Material characterization result for 3D mode

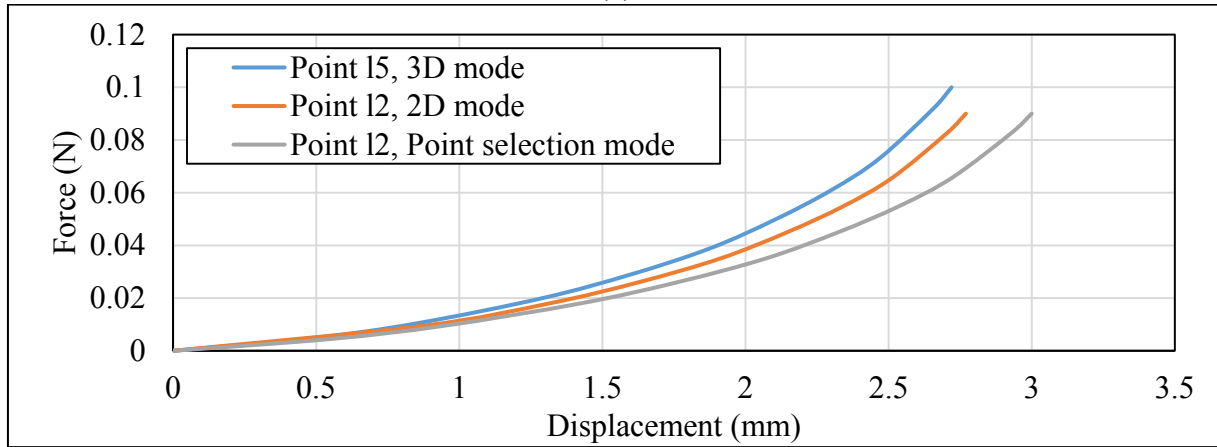
Material	Point	R_{in} (mm)	Calculated R_t (mm)	Calculated i (mm)	Calculated F_n (N)	E (KPa)	Average E (KPa)
Liver	l_4	6	132.4	2.91	0.12	1.9	1.7
	l_5			2.72	0.10	1.6	
	l_6			1.98	0.06	1.5	
Kidney	k_4	6	72.3	2.92	0.31	12.2	11.7
	k_5			2.76	0.28	11.8	
	k_6			2.60	0.25	11.2	
Atrial	h_4	6	41.7	2.92	0.63	47.7	43.0
	h_5			2.68	0.51	40.4	
	h_6			2.31	0.41	40.8	

The result of 3D mode characterization shows that there is another significant change between measured magnitudes in 3D and 2D modes. Measured indentation is decreased 13.9% for point l_6 and 3.7% for point k_6 in comparison to the 2D mode. This value is increased by 4.5% for point h_6 on heart tissue. The measured F_n is also decreased 3.7% for k_6 and 20.5% for h_6 . There is no change for measured force at l_6 (see Table 4). As a result, the calculated E has a significant change specifically for the points that are located on curved parts of the tissues. The calculated E has a significant decrease of 0.5 KPa (50%) for point l_6 , 11 KPa (36.9%) for h_6 and 0.7 KPa (6.7%) for k_6 . These results indicate that the curvature of tissues, along with precise depth calculation, plays an important role in tissue characterization on the natural shape of the organ using tactile sensors. In Figure 23, the captured F_n versus measured effective applied displacement on liver are illustrated for the each mode of material characterization. The measurements are done for $l_1 \dots l_6$. The point l_1 and l_4 are located on the same curvature, similarly

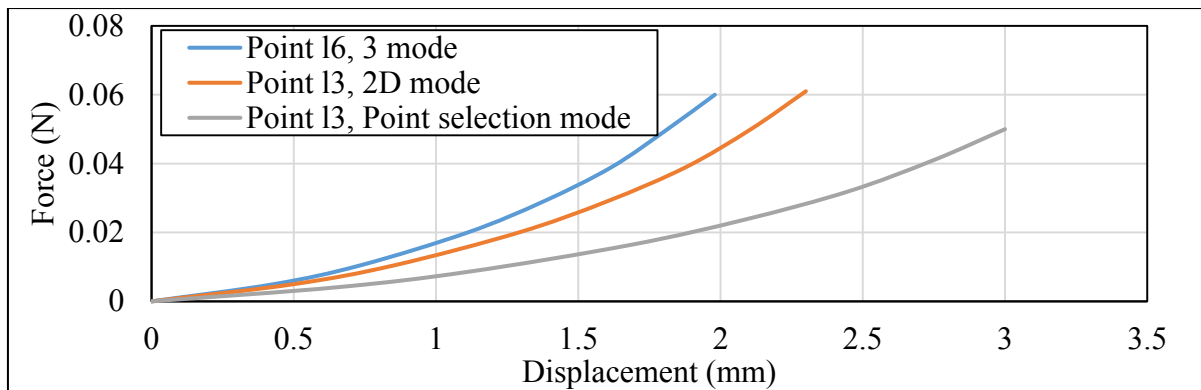
l_2 and l_5 , and pair of l_3 and l_6 . Indentation occurs on point 1, 2 and 3 in 2D mode, and on points 4, 5 and 6 in 3D mode.



(a)



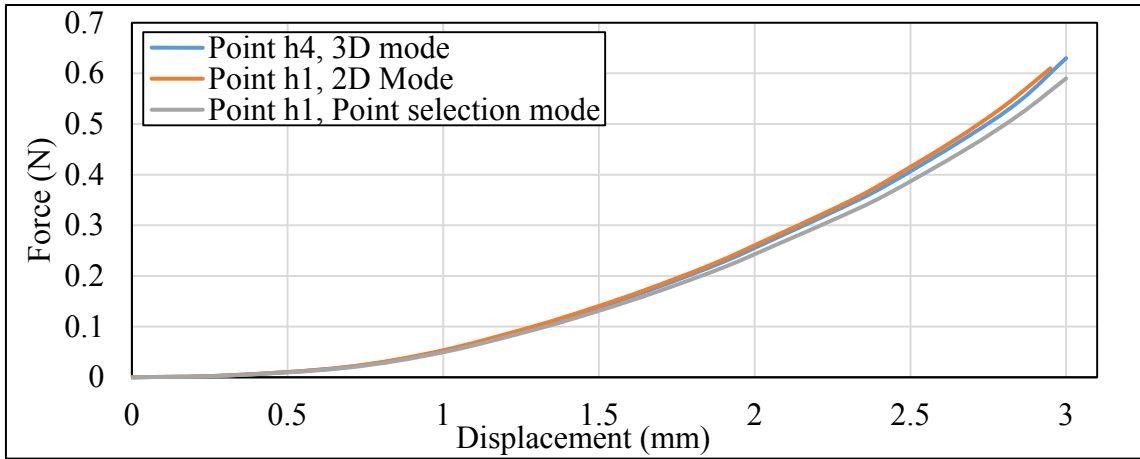
(b)



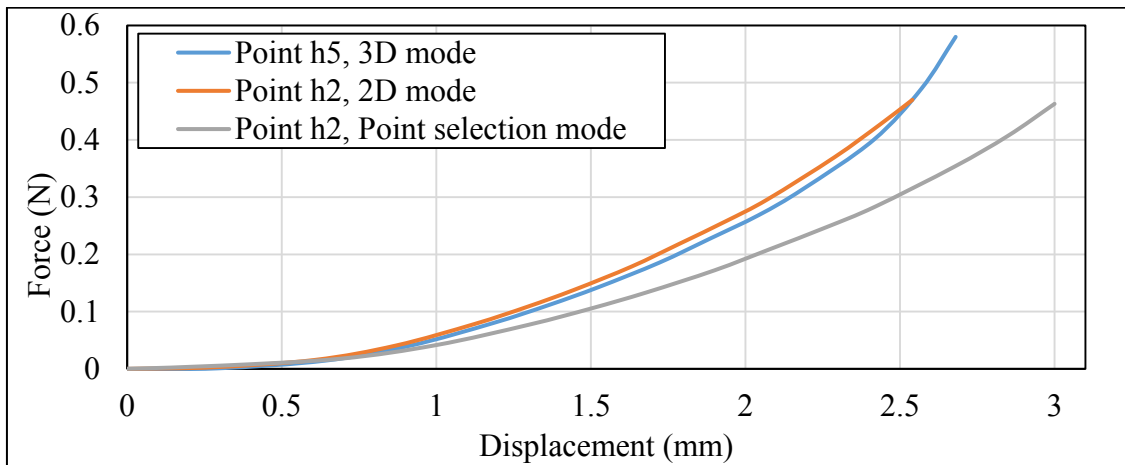
(c)

Figure 23. Captured force (F_n) versus measured effective indentation (i) on liver tissue in spot selection, 2D and 3D mode for points (a) l_1 and l_4 (b) l_2 and l_4 (c) l_3 and l_4

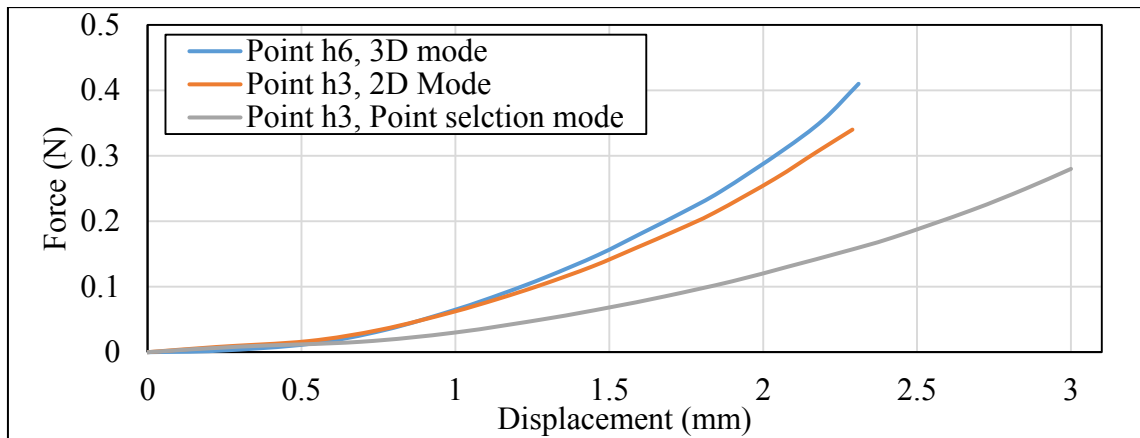
It can be seen that when the radius of curvature decreases, the force-displacement relation significantly changes amongst three modes. Since calculation of normal interaction of surface and depth of indentation can be calculated more precisely in 3D mode, material characterization is more accurate relative to other modes. As a result, the calculated E in 3D mode is reliable for all parts of the tissue. The 2D mode can be used to get accurate result on curvature with a radius larger than 150 mm, and the point selection mode can be used on flat parts of the tissue. The captured force and calculated indentation for atrial tissue for the specified points of Figure 21 (e) can be seen in Figure 24. The results show that the proposed method calculates elasticity modulus for the atrial tissue which is 25 times harder than liver.



(a)



(b)



(c)

Figure 24. Captured force (F_n) versus measured effective indentation (i) on liver tissue in spot selection, 2D and 3D mode for points (a) h_1 and h_4 (b) h_2 and h_5 (c) h_3 and h_6

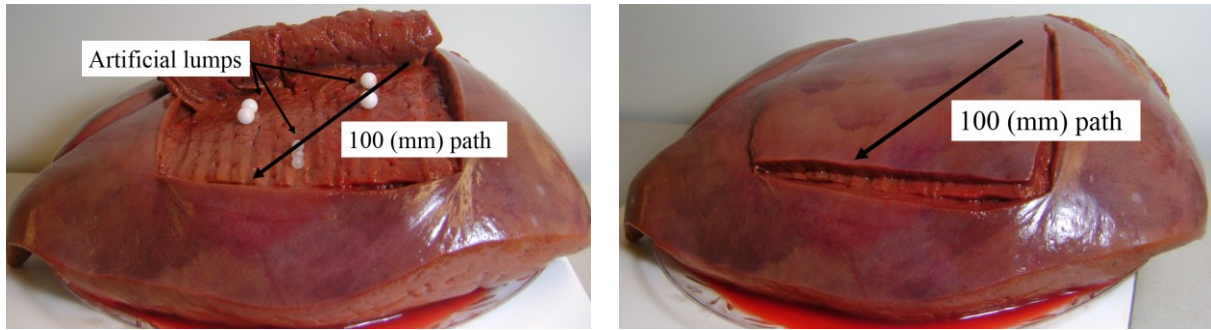
The average magnitude of elasticity modulus for the three points which are measured in 3D mode is calculated and shown in Table 5. The average value is compared with the modulus of elasticity for bovine liver and kidney in the literature which is shown in Table 6. The large variation is due to different testing conditions such as post-mortem time and temperature differences [82]. However, the calculated values comply with those mentioned in literature.

Table 6. Modulus of elasticity for bovine liver and kidney in literature

Reference	Tissue	E (KPa)	Methods/comments
Current research	Bovine liver	1.7	Calculation of modulus of elasticity according to Hertzian contact theory with spherical indenter
Reiter <i>et al.</i> (2014) [83]		1.18	Loading response of a static indentation is used to calculated best linear fit of the curve's initial response
Ayyildiz <i>et al.</i> (2015) [84]		0.801	Linear elastic modulus is estimated by $E=3\mu$, where μ is linear shear modulus of material and calculated by optimization of material. It is assumed that the liver is homogenous, isotropic and incompressible material.
Ocal <i>et al.</i> (2010) [85]		5	Long term elastic modulus estimated in 1-4 hours after demise
Yarpuzlu <i>et al.</i> (2014) [86]		1.5	Linear elastic modulus which is calculated in 5 hour preservation time using static compression indentation
Current research	Bovine kidney	43	Calculation of modulus of elasticity according to Hertzian contact theory with spherical indenter
Recouvreux <i>et al.</i> (2011) [87]		64±7	Mean elastic modulus of bovine kidney
V. Egorov <i>et al.</i> (2008) [88]		38±7	Calculated Young's modulus with developed tissue elastomer which measures modulus of elasticity with spherical indenter loading curve

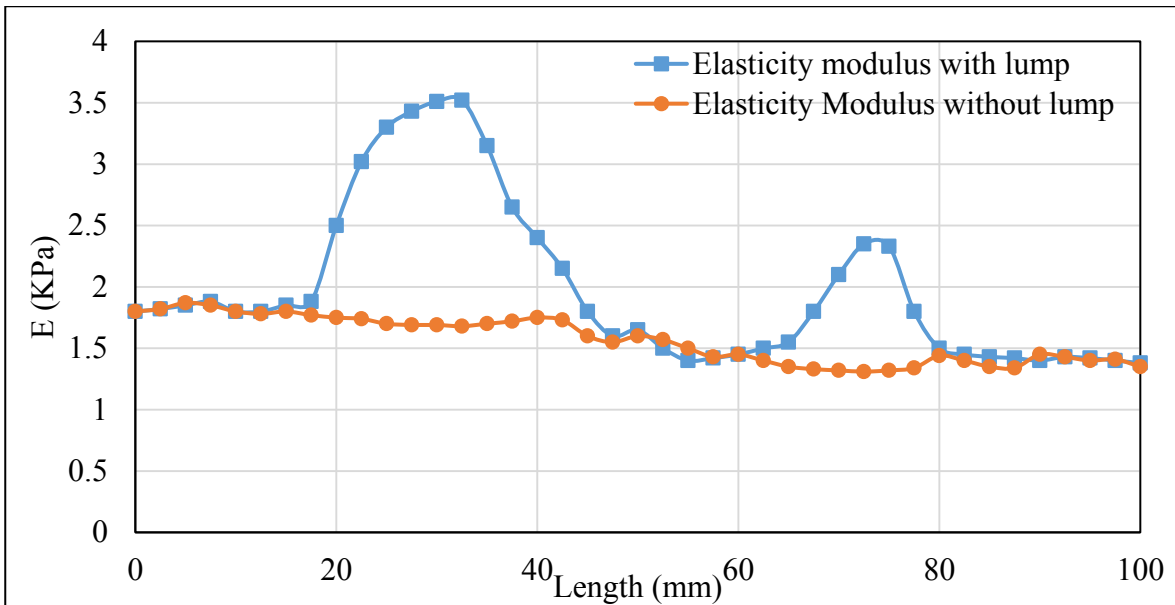
Calculation of elasticity modulus using developed method in current study allows users to locate the points on tissue with different hardness. This feature enables the system to find the location of buried lumps which, in tissue, changes the surface interaction between sensor and tissue. By knowing the surface geometry which is obtained by STA, the ball caster can be rolled on a

material surface to map relative softness. For this aim, the liver specimen is cut with a 20 mm layer thickness as shown in Figure 25(a). The plastic balls that substitute for artificial lumps are placed in a certain position. The plastic balls have 7.8 and 4.7 mm diameters. Afterwards, to obtain the 3D surface of the liver, the ball is rolled on the surface with a fixed prescribed indentation on the material surface. The start and end points of the motion is defined by the user. The 100 mm long path is defined for the motion with a 3 mm indentation on the surface of material as shown in Figure 24 (b). As the sensor is rolled on the surface, the material elasticity modulus is continuously calculated for predefined motion. The calculated modulus of elasticity for the linear motion is shown in Figure 25(c). The results are shown for every 2.5 mm distance on the traveled path. The two captured peaks indicate that the two points are harder than the other parts of the specimen. The positions of the harder points are saved and illustrated to the user as the location of the lumps.



(a)

(b)



(c)

Figure 25. (a) Artificial plastic lumps which are buried in depth of 20 mm from tissue surface (b) 100mm pre-defined maneuver for lump detection (c) Calculated elasticity modulus of tissue which is selected by 2.5 mm distance for the lump detection

The resulting 2D and 3D surface profiles (as shown in Figure 21 and Figure 22) illustrate a larger area of the goal surface for a better understanding and demonstration of the proposed method. In reality, however, one or two loops of spiral motion around a desired point is sufficient to calculate surface profile characteristic which is the basis of the material characterization process. Consequently, the time of scanning around the desired point will be acceptable for real-time material characterization.

Chapter 3 - A new tactile array sensor for viscoelastic tissues with time-dependent behavior

3.1 Introduction

The major motivation for developing the sensor in our proposed method was to compensate for the deficiencies inherent within current minimally invasive surgery (MIS) systems. During RMIS, a surgeon using the master controls of the surgical apparatus initiates commands which are transmitted to a probe inside the patient. Since the surgeon operates from a remote location, he loses the perception that is usually obtained from direct touch and palpating the patient's tissue [13, 89, 90]. Current reviews of articles show that although tactile sensors are being developed by researchers using piezoelectric, piezoresistive, optical and pneumatic transduction principles, the variety of data collected by these sensors is very limited in scope. Specifically, these new tactile sensors are capable to collect force and displacement data by directly touching a tissue. This data is used to obtain compliance and hardness information, which are a function of the sensor geometry, structure, and measurement pathways [58, 91, 92]. In most cases, these sensors have not been put into use outside the laboratory and read strictly pressure and force mapping by direct tissue contact.

In this research, a new type of tactile sensor is proposed for surgical applications. It can be considered as being a new generation of tactile sensor which can extract the indentation and displacement rate in addition to measuring force and displacement. This added capability can also be beneficial in other applications such as for use in robotic arms and humanoid robots. Tactile sensors play an important role in accomplishing various functions of humanoid robots such as object manipulation [49, 93], robotic hands [93-95], decoding and transferring tactile data collected in the fingerprint area of humanoid robots [96, 97], and classification of human facial features [98]. Also, communication between a robot and a human can be performed for different purposes such as in the nursing context [99], socializing and affective touching [100]. Recently, many types of tactile sensors have been developed for use in robotic arms and graspers. Dahiya *et al.* developed a polyvinylidene difluoride matrix of tactile sensors for robotic grasping application [101]. Their developed tactile sensing chip is able to measure the dynamic

contact force in a robotic application. Aoyagi *et al.* in a similar research work developed a matrix of capacitance sensors-embedded in Polydimethylsiloxane (PDMS) for use in robotic applications. They used a neural network algorithm that compared the output of different sensors to estimate the components of the contact force in the x, y, and z axes [102]. Considering the different functions of humanoid robots and human interactions, it is highly challenging to develop a tactile sensor that can capture even more information during such an interaction. The compatibility of this proposed sensor for use in a humanoid robot can be studied from two major aspects. Firstly, the characteristic of any material that is touched relative to time is explained in detail in the Sensing Algorithm Section. Secondly, the similarity in the trapezoidal shape of the sensor to a human fingertip makes it simpler to replicate it during touch. As illustrated in Figure 26, the trapezoidal dimensions of the sensor can be modified according to the index finger or thumb on humanoid robots.

Another application of the sensor can be as a substitute for the finger for palpating tissues. Ever since the era of Hippocrates to the present day, palpation using the finger has always been used as an initial step to locate the existence of possible abnormalities [103]. As an alternative to the human finger, any probe that is capable of determining material properties accurately would be of great assistance when wishing to make an accurate diagnosis. Such an innovation would be of great help to specialists in order to determine the presence, location and properties of tumors. Filloy *et al.* [104] have demonstrated a probe that is able to quantify the modulus of elasticity in a controlled indentation. Ayyildiz *et al.* [105] have compared their developed compact tactile sensor with a human finger for the purposes of detecting a breast lump. They have shown that while a human finger's performance is slightly better in shallow inclusions, a tactile sensor can operate more efficiently in deep inclusions. In order to detect abnormalities, these types of probes improve the specialist's manual dexterity since they can be applied non-invasively, compared to previous radical biopsy procedures.

The applications of tactile sensors in the context which viscoelastic materials are in direct contact with the sensor such as RMIS, non-invasive cancer detection probes, and humanoid robots show significance of developing a sensor that is capable of determining viscoelastic characteristics of materials. Viscoelastic model of a tissue represents the most realistic behavior, which clearly demonstrates time dependent mechanical properties of live tissues. As a result, the sensor should

be able to capture spatio-temporal response of the viscoelastic materials. Many efforts have been made to increase the high spatial resolution and precision of the robot sensor, such as distributing an array of tactile sensors on the contact surface using composite piezoelectric materials in order to interact with the external environment [106]. Even using quantum tunnel composites, tactile sensors still possess spatial resolution comparable to the human fingertip, which is 1mm, so it still remains a challenging task to increase this temporal resolution, especially during the dynamic mechanical interaction between the sensor and touched surface [107, 108]. A Fuzzy algorithm was designed to identify type of different artificial tissues based on duration of time which takes for stress relaxation as a unique characteristic in the indentation procedure [32]. They added this time-dependent feature as an input to the detection algorithm in addition to stress and displacement. The stress was measured by a strain-gauge and the displacement was controlled by a robot during the indentation procedure.

However, soft tissues tend to exhibit nonlinear deformation with time and deformation-rate dependency. Basdogan [30] showed that dynamic loading and response in both the time and frequency domain resulted to obtaining accurate mechanical properties of human and animal livers. Sumur *et al.* [31] also investigated that indentation with different speeds led to record different forces for their soft specimen tissues, specifically bovine liver. These forces were recorded and used in deriving Maxwell, Kelvin, and other models of viscoelastic materials. As mentioned above, in tissue related applications, extra parameters in relation to viscoelastic behavior of tissues can be measured to add more certainty to the sensor output. The new parameters that can be measured are force and displacement measurements, the force rate and displacement rate which can be taken into account by virtue of the time-dependent response of viscoelastic tissue to stress or strain. If a constant strain rate is used between readings, the differences between two different tissues will be more clear and reliable.

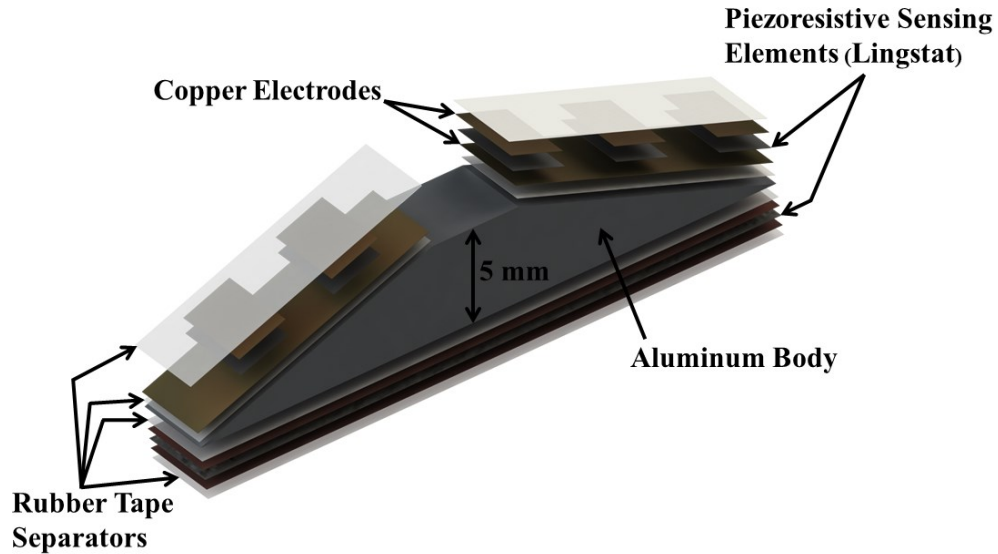
Our experiments show that a single tissue manifests a different force-displacement behavior for different displacement-rate applications. In order to distinguish among various tissues using force-displacement behaviour, it is therefore necessary to monitor and control the force rate and the displacement rate. A new generation of tactile sensor design based on array sensors may answer this need. The new design will be able to pick-up force application rate as well as

displacement rate, in addition to basic force and displacement measurements. The former two data sets of interest are crucial to obtain a soft tissue's relative viscoelastic behaviour.

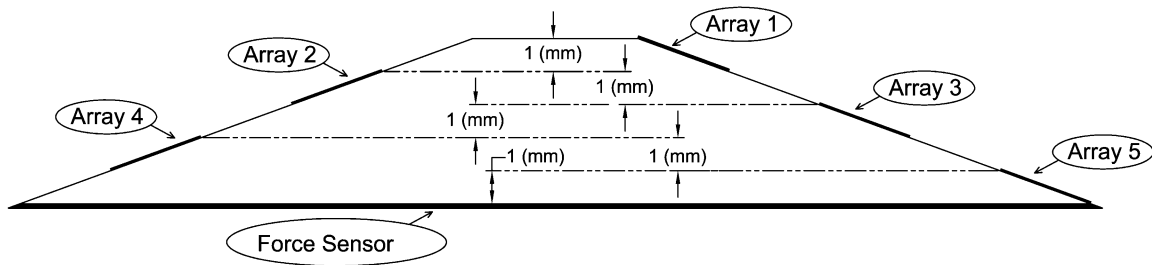
The sensor described in this research was designed because all current literature on tactile sensors appears to show that they only measured the contact force/pressure during the actual touch. For example, in two recent researches [96, 109] they state that there is lack of tactile sensors that are suitable for determining the difference between viscoelastic materials. The novel feature of the sensor described in this research, unlike previously developed sensors, is that it is capable of distinguishing the difference between several soft tissues with viscoelastic behavior.

3.2 Sensor Structure Design

In this section, the overall design of a piezoresistive tactile sensor is explained. Using piezoresistive material as a force transducer, and placing pieces of the material strategically, the sensor is able to provide the necessary information to obtain the time-dependant behaviour and hardness of tissues. An array of electrodes bonded to an inclined plane relative to the surface of the tissue, and facing the surface of the tissue, act as triggers. Once contact is made between the tissue surface and one of the electrodes, the main force sensor is signaled to record its immediate force value. An exploded schematic configuration of the tactile sensor is shown in Figure 26.



(a)



(b)

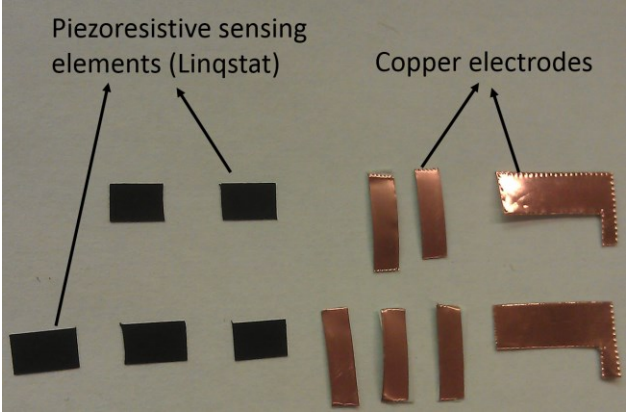
Figure 26. (a) Schematic exploded view of the sensor and its components (b) Side view of sensor with indenter pointing upward

The array of fixed piezoresistive triggers is key to the acquisition of consistent force-displacement-time data. The height of the indenter is exactly 5 mm, allowing five electrodes to be placed at 1 mm height intervals. The electrodes are placed on alternating sides such that the size of each electrode is maximized without overlapping adjacent electrodes.

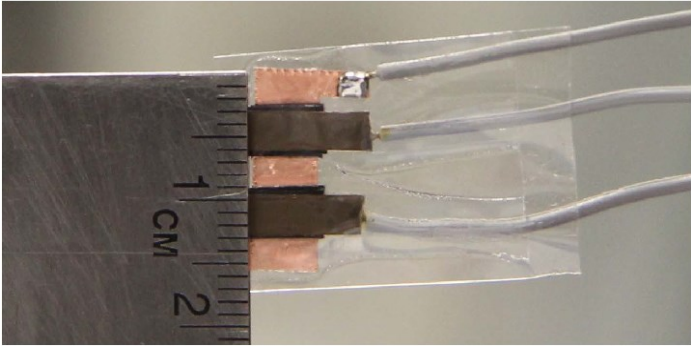
3.3 Sensor Fabrication

The sensor has a simple construction composed of several sensing elements bonded to a central trapezoidal piece. The two array sensors consist of piezoresistive sensing elements symmetrically sandwiched by a copper electrode layer and a polyester film or silicone tape as

shown in Figure 27; symmetrically sandwiched means that there is the same layer above and below the sensing element [33]. The location of each sensing element in the two array sensors on the trapezoidal body is critical to proper data acquisition using the indenter. The trapezoidal plate could be made from steel, aluminum, or any rigid material.



(a)



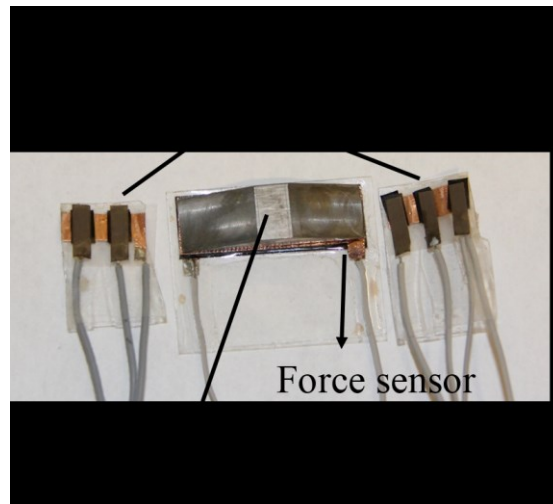
(b)

Figure 27. (a) Components of array sensor (b) The fabricated array sensor size

After fabrication of the individual components of the array tactile sensor, the elements are adhered together to form the tactile sensor as shown in Figure 28(b).



(a)



(b)

Figure 28. (a) Manufactured components of the array tactile sensor (b) Fabricated tactile Sensor

The sides of the trapezoidal body piece have an angle of 20 degrees with respect to the base of the piece. The angle was chosen based on experimentation. It allowed for a workable balance between array sensor to tissue contact, and vertical distance between sensing elements. Since time, force, and displacement are simultaneously recorded based on defined contact threshold, a sizeable spacing between readings is desired. The indenter's electrical circuit is based on that described by Kalantari *et al.*, and was adapted for the array sensor [33].

3.4 Sensing Algorithm

The novel sensing algorithm depicted in Figure 29 is relatively simple and has many useful features used to determine tissue properties. It was developed in the LabView environment and was designed for use on the array tactile sensor.

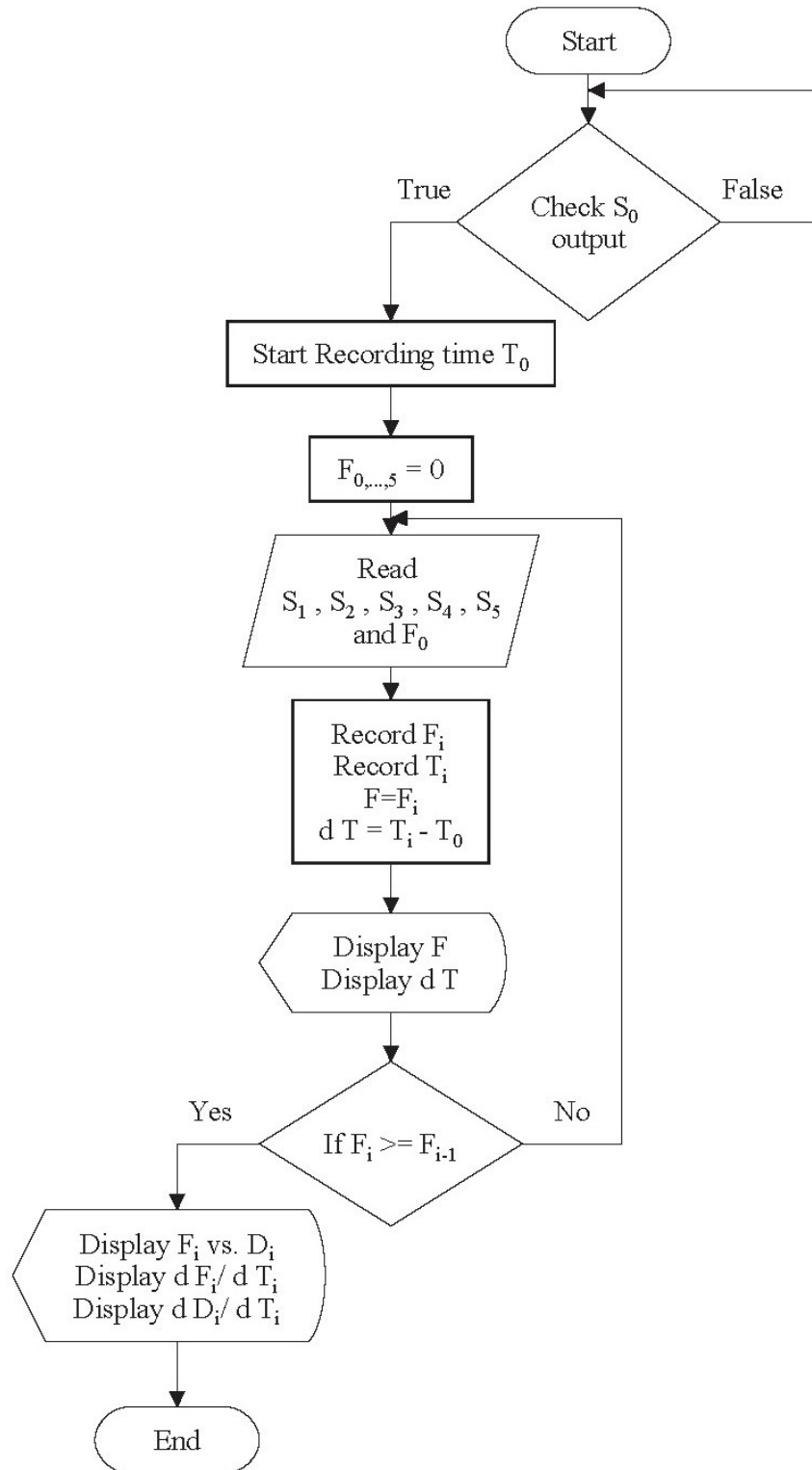


Figure 29. Sensing flowchart for tactile sensor [110]

The sequence begins when a contact is made between tissue and sensor. That is, when the force measured by the sensor is greater than null. The main force sensor was calibrated to have a low threshold value since initial contact force may be quite small. This is possible due to the low noise generated in the piezoresistive material; a threshold is used mainly to subdue the influence of noise signals. Figure 4 shows how the output force is constantly being measured. Once the sequence is triggered by a non-zero force measurement, the time recording begins. Each time a successive sensing element detects contact, the force measurement and time is recorded until the 5 mm indentation depth. It can be considered that:

$$F = F_i, \text{ and } \delta T = T_i - T_{i-1}$$

Where F_i is the instantaneous force measurement for $i = 1, 2, \dots, 5$, and dT is the time between recordings in the i^{th} step. A total of five dT are recorded. For a full indentation run, the average displacement rate can be recorded by dividing the depth of travel by the summed up the recorded five T_i measurements, as shown in Eq (9):

$$\bar{V} = \frac{5}{\sum_{i=1}^5 T_i} \text{ (mm/s)} \quad \text{Eq (9)}$$

where \bar{V} is the average displacement rate (average velocity).

It is important to note that the output of each of the sensing elements as well as the main force sensor is constantly being monitored. To distinguish between useful data, such as that obtained during loading-shift registers used in the program, the monitored output from the elements, at time N , is continuously compared to previously recorded values, from $N-1$, and a redefined threshold value. The sensing element is considered to be in contact with the tissue only when the output at time N is greater than that at $N-1$, and it is greater than the threshold value. The value of force for each of the sensors is computed from their output voltage in the same way, since they are all made of the same materials. The change in output voltage of a sensor is proportional to the change in applied force according to a calibration procedure [33].

3.5 Experiments

The equipment used to test the sensor array is shown in Figure 5.

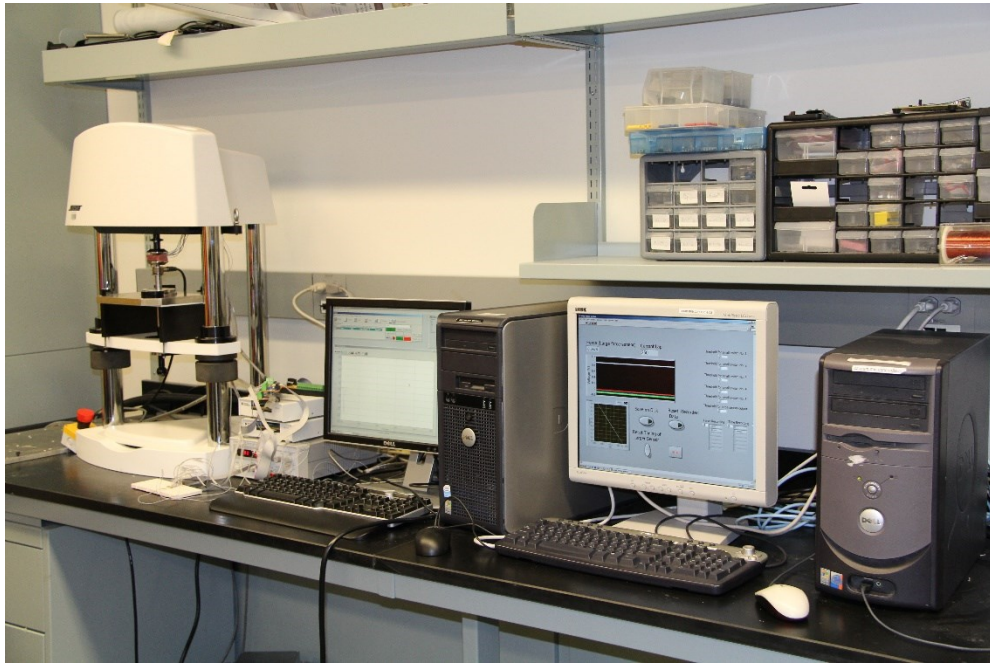


Figure 30. Equipment used to test the tactile sensor array

The size and type of the tissue used to test the indenter are found in Table 7. Once the tissues are received, they were cut into uniform rectangular specimens, such that they would be of appropriate size for testing equipment.

Table 7. Tissue types and dimensions

Tissue	Tissue Type	Dimensions (mm)		
		Length	Width	Height
1	Atrial tissue	44	25	14
2	Bovine vastus lateralis muscle			
3	Bovine liver			

The selected tissues were bovine vastus lateralis muscle, atrial and liver tissue. Brown *et al.* [111] showed that the elastic response of tissue for porcine liver is almost the same within three hours post-mortem. In the current project, timing of indentation experiment tests were designed

in such a way that all data recordings were made within that three-hour period. Since data collecting procedure involves indenting the material surface, specimens lose interstitial water after each indentation procedure. This dehydration results in the hardening and stiffening of the material [59]. To prevent the effect of this phenomenon on experiments, several samples from each tissue are prepared and each sample was only used once for the indentation test. In order to have comparable results between runs, the sizes of the tissue specimen were kept uniform. The calibration of piezoresistive sensors for the purpose of connecting them to a written code is an advanced research topic of its own [33]. It is not discussed in detail here because it is considered to be outside the scope of this thesis. The ElectroForce Bose 3200 was used for applying indentation on surface of material and also for verifying the measured output of the tactile sensor. This device is specifically designed for material testing applications by Bose Corporation. This equipment is capable of applying strain and stress to within an accuracy of one micro meter and Newton, accordingly.

As shown in Figure 31, the device has fixed and moving jaws on top of each other. The upper jaw moves and applies displacement to the top surface of specimen. Figure 31 shows the progressive indentation of the tactile sensor into the tissue in which the upper jaw has pushed the sensor towards the tissues from the top. The sensor is attached to the upper jaw of the ElectroForce Bose, and the tissue is placed on the lower fixed jaw. Each tissue is subject to a penetration depth of precisely 5 mm by the tactile sensor.

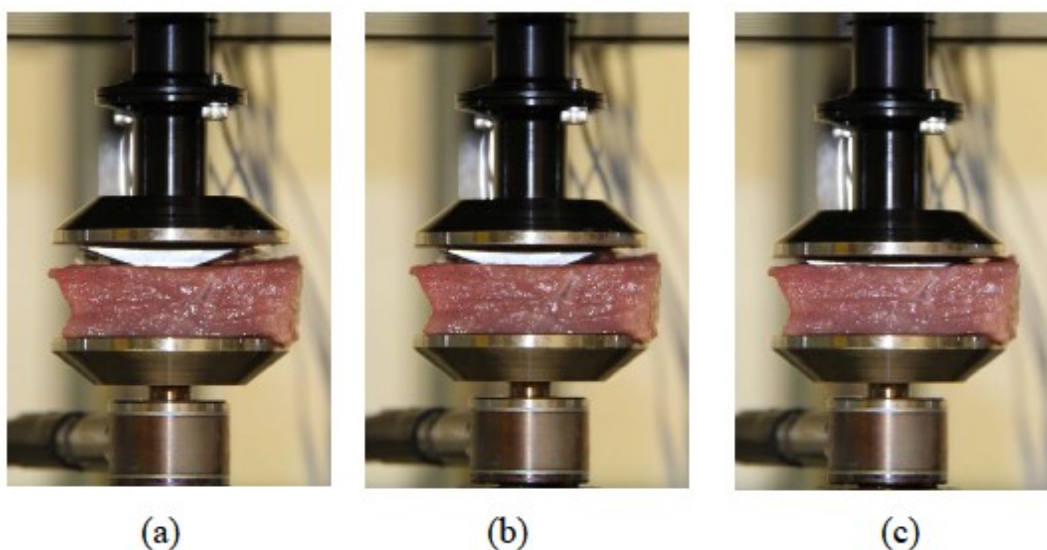


Figure 31. Progressive indentation of the tactile sensor into the tissue

During these experiments, the measurements were conducted on each tissue several times at different displacement rates. The experimental results clearly validate the concept that the force-displacement data of soft tissues, which is highly dependent on the displacement rate of the indenter. This data could be compared when the average velocity displacement and force in the tactile sensor during indentation have been recorded. Figure 32 shows the graph of the experiment conducted to obtain measured data of atrial tissue, tissue No.1, at different displacement rates.

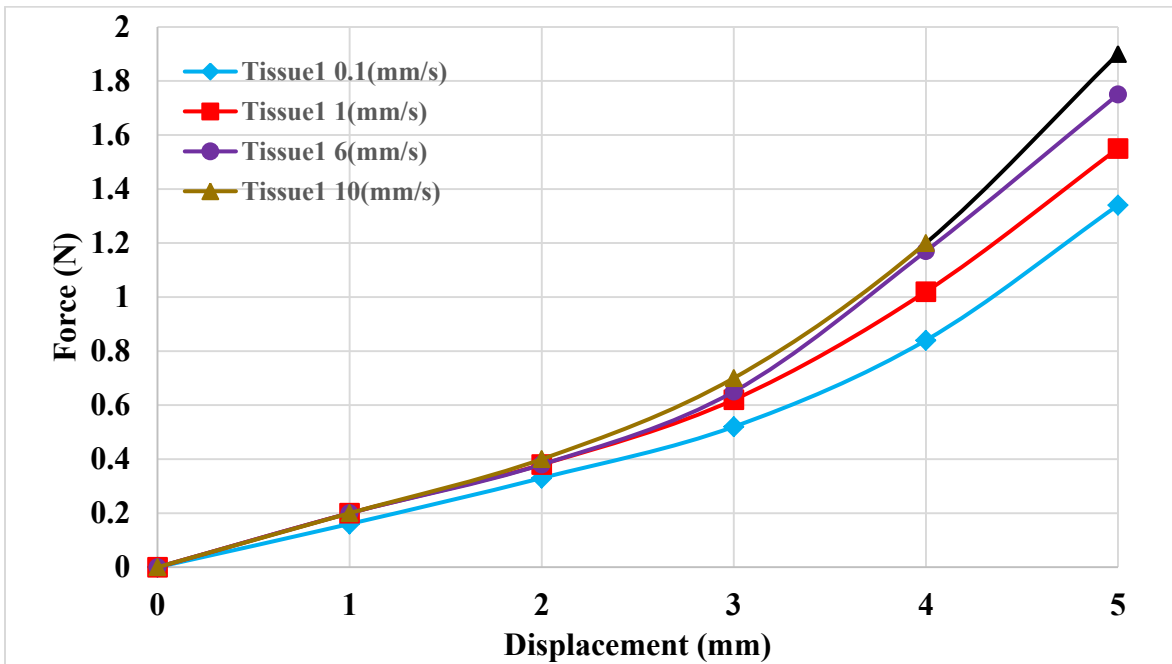


Figure 32. Force-displacement response of tissue 1 (atrial) for different rates

The graphs in Figure 7 show that the displacement rate can change the tissue response to force or displacement. In order to validate the results, two indentation rates of 0.1 mm/s and 10 mm/s were chosen. Then, the ElectroForce Bose is programmed to apply a 5 mm indentation by the upper jaw on the surface of each tissue with the two selected indentation rates. During these experiments, the force applied was recorded by the ElectroForce Bose sensor during indentation. Comparison of recorded data by the sensor and ElectroForce Bose reveals that the proposed array sensor can be applied for a wide range of indentation rate.

Figure 33 and Figure 34 show that as the depth of indentation (and consequently applied force) increases, the difference between the output of the sensor and forces produced by ElectroForce

Bose decreases. This error can be caused due to the nature of piezoresistivity since the output of the piezoresistive sensor is nonlinear at the moment of contact due to large resistivity when no force is being applied.

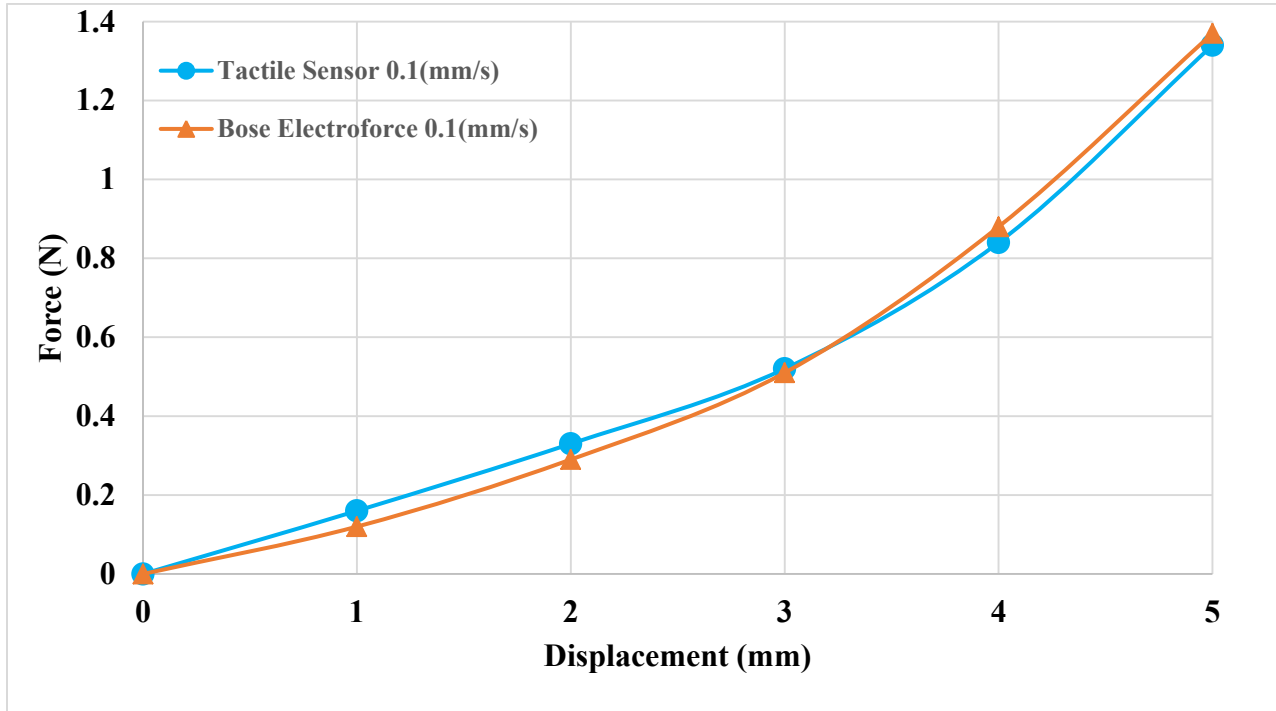


Figure 33. Comparison of the measured force of the array sensor and ElectroForce Bose 3200 for tissue 1 with an indentation rate of 0.1 mm/s

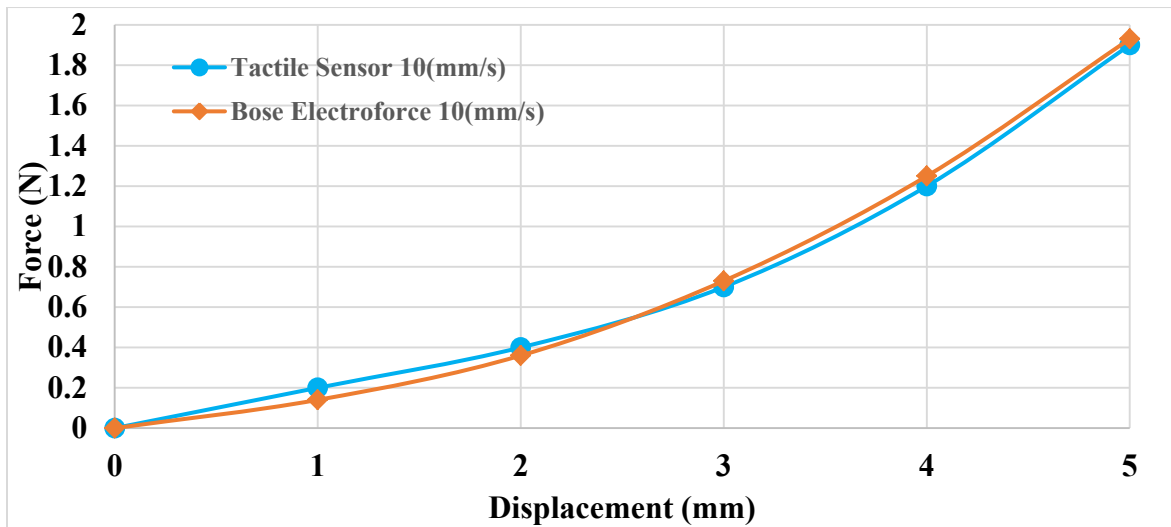


Figure 34. Comparison of measured force of array sensor and ElectroForce Bose 3200 for tissue 1 with indentation rate of 10 mm/s

Evidently, the force-displacement dependence on displacement rate existed for each tissue, but with varying degrees. In another experiment, the response of three tissues was compared at uniform displacement rates and for three different rates. For example the data in Figure 35 is shown for a displacement rate of 0.1 mm/s.

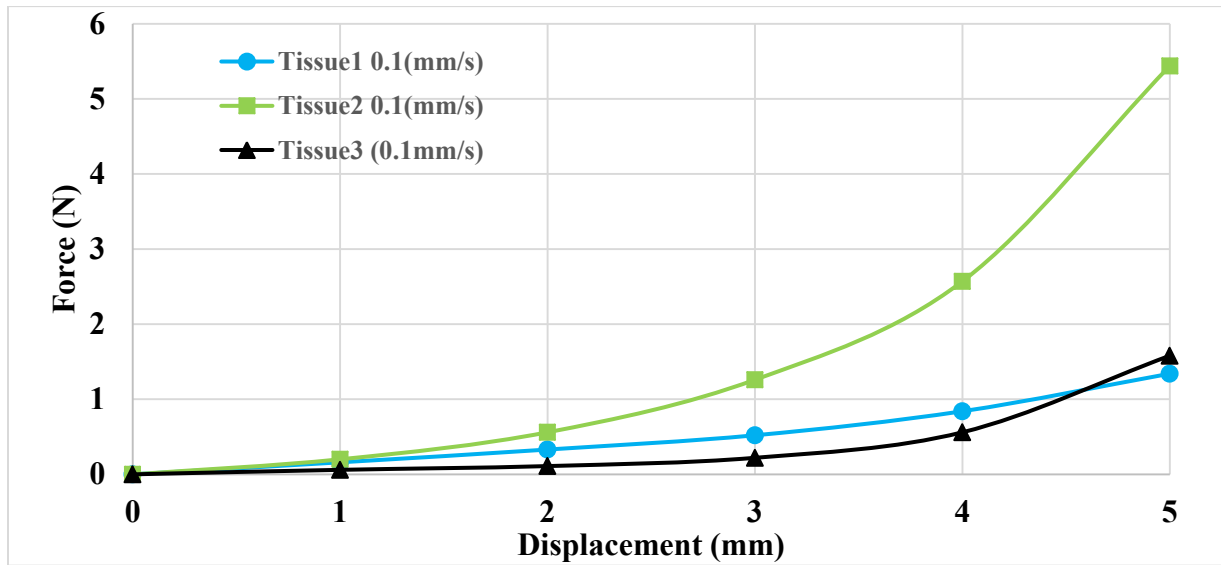


Figure 35. Result of tactile sensor on three tissues at an indentation rate of 0.1 mm/s

The results show that tissue 2 is harder than tissue 3; and tissue 3 is harder than tissue 1 at a displacement rate of 0.1 mm/s. Interestingly the behavior of tissue 1 and tissue 3 became more identical when the indentation rate increases to 1 and 10 mm/s.

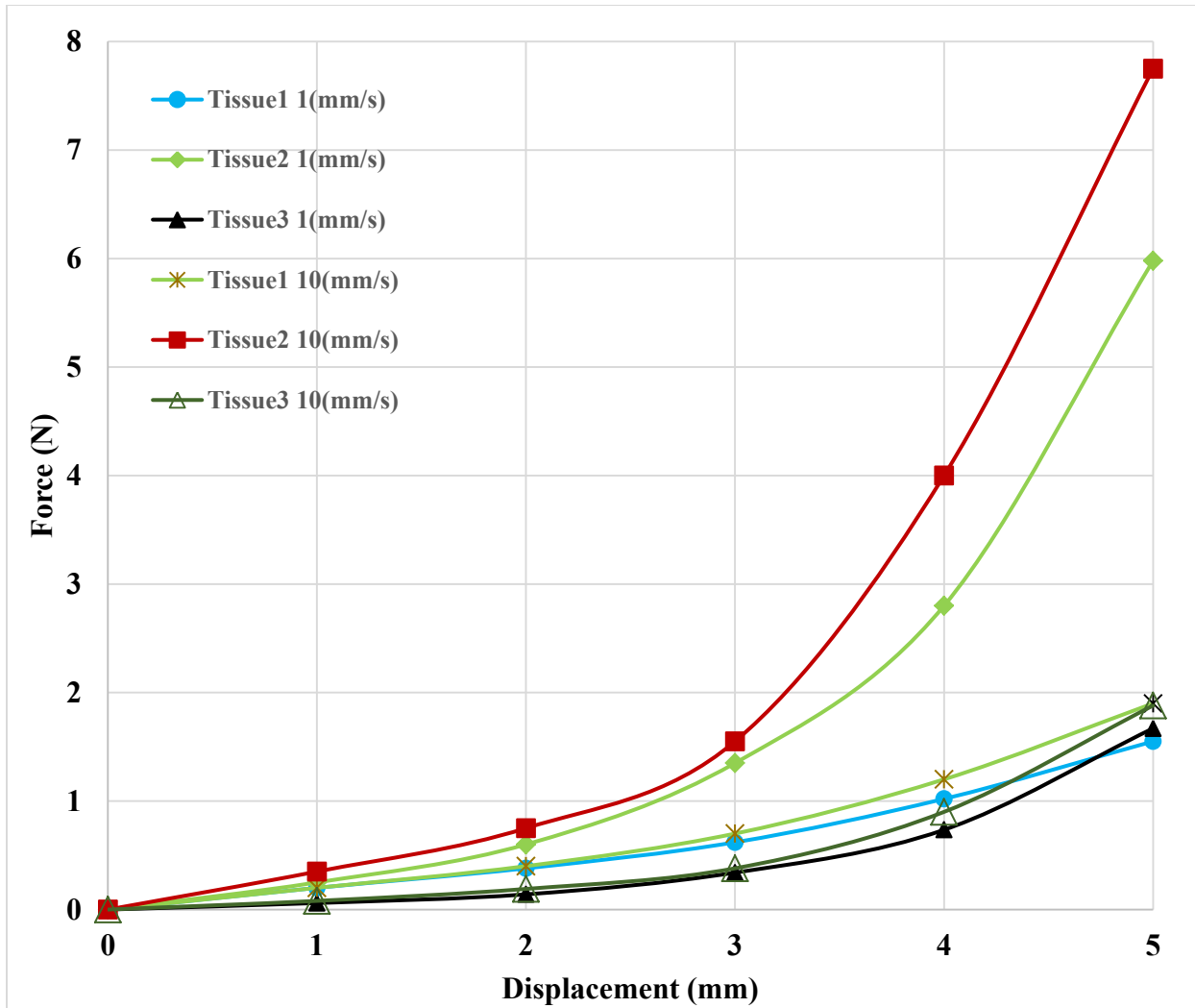


Figure 36. Result of tactile sensor on three tissues for 1 and 10 mm/s indentation rates

As shown in Figure 36, there is a small difference between the final force value of the sensor at an indentation rate of 1 mm/s but, when the sensor is pressed on the tissues at the maximum rate of 10 mm/s, the final value is almost identical. This phenomenon clearly shows that recording the indentation rate, in addition to the force and displacement feature, assists in distinguishing between different viscoelastic materials. In this case, for example, the value of 1.88 N is recorded for two different materials, tissue 1 (atrial) and tissue 3 (liver) at an indentation rate of 1 mm/s. This resulting value occurs due to the fact that two different trends are being measured concurrently by this newly developed sensor. As a result, and by knowing the history of force in

previous steps that is recorded by proposed sensor, we can determine which material is being touched by the tactile sensors.

Another significant point in the experiment is the sudden change in captured force by increasing the indentation depth from 4 to 5 mm for tissue 1 and tissue 2. As the depth is increased to 5 mm, it can be seen in the final steps that these two tissues are similar in behavior. In fact, this situation is the same in reality. For example, the harder one pushes with the finger, the more difficult it is to distinguish between the degrees of softness of two objects having a similar response. Experiments showed a notable change in tissue behavior for different displacement rates. For example, the response of tissues 1 and 3 varied drastically between displacement rates of 0.1 mm/s, 1 mm/s and 10 mm/s. Tissue 1 showed a predictable trend during the initial steps while tissue 3 showed harder property. Considering all the results, it can be concluded with certainty that tissue 2 is harder than tissue 1 and 3 although, however, the difference in hardness between tissue 1 and 3 can be determined based on the displacement rate. This experiment showed that the displacement rate is a determining factor when distinguishing between the degrees of hardness of materials possessing similar viscoelastic properties.

A novel tactile softness display was developed by Dargahi *et al.* [112] that produces the softness of tissues based on mechanical properties of touched material. As shown in Figure 37, the linear actuator regenerates the softness of nonlinear materials using a predefined algorithm which is achieved experimentally from the strain-stress test. The force sensor transfers the measured pressure on its surface, and the actuator changes in length as the original material is touched. As shown in Figure 36, the determining factor in sensing softness is the *rate* at which force is applied when indenting viscoelastic materials [112].

In Figure 37, substituting the illustrated sensor (which can be called the “non-rate dependent” sensor) with the proposed tactile array sensor can be considered a feasible application of the developed sensor. For example, if the stream of data that comes from the array sensor is set as the force input of the illustrated algorithm, the touchable actuator will mimic the behavior of viscoelastic material by considering the rate of indentation. As a result, the sense of touch can be recreated simultaneously even though the surgeon has no direct physical access to the target tissue.

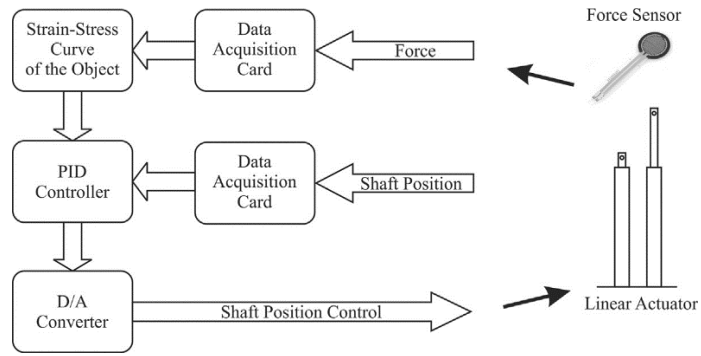


Figure 37. Regeneration flow chart of softness for nonlinear materials [112]

Chapter 4 - Conclusion and future work

In Chapter 2, the proposed method was shown to satisfactorily perform material characterization and abnormality detection of a naturally shaped organ. Therefore, the approach can be used to measure the in vivo characteristics of solid organs specifically during RMIS using a tactile sensor. It is also shown how the forcing element of the tactile sensor, which is usually utilized to capture forces, can also be used to provide a 2D or 3D shape of the goal tissue. To this end, an admittance control approach is used to control the position of a robot using tactile force feedback.

In chapter 3, the novel idea of recording time during touch was provided in the form of a new array tactile sensor. An array tactile sensor was conceptualized, designed, and manufactured for RMIS application. To that effect, a new algorithm was developed to monitor and record the force, displacement, and time during indentation. The algorithm also processes that data into average displacement rate. Experimental force-displacement curves showed that the new sensor is able to distinguish degrees of hardness of various tissues that exhibit viscoelastic properties. The experiments also provided evidence to a need for such a sensor due to the sensitivity of tissue response to indentation displacement rate. In addition, the need was discussed to measure the displacement rate at the moment that contact is made between the sensor and the tissue. Such an array tactile sensor could inspire a new generation of tactile sensors for robotic applications, which demand knowledge of a soft tissue's viscoelastic properties, a feature beyond the capabilities of existing sensors.

Our future work will focus on two major goals. First, the developed system will be integrated with a recently developed tactile sensor, which is capable of characterizing live tissues with respect to the spatio-temporal response of the viscoelastic materials; thus, the mechanical characteristics of live tissues will be analyzed in terms of the tissue's time-dependent properties. Second, the current admittance control will be improved to stabilize contact force not only for static points, but for oscillating contact points as well; oscillating points are result of the natural heart beat or human aspiration. In this condition, the force feedback control should track the oscillating contact points to get the surface profile of tissues. The indentation on the tissue's surface will be applied through phase lag/lead between the force sensor and beating organ. A

preliminary study showed that the developed system can stabilize a contact on one surface contact point. Tests are scheduled, where an artificial beating phantom will be replaced with current silicon-rubber materials. The proposed closed-loop artificial palpating system can be used for both material characterization and lump localization [113].

Another future work is the parametric study and sensitivity analysis of buried lumps during indentation tests. The relation between location and size of lumps can be discussed based on the pre-calculated force distribution in finite element analysis (FEA). The calculated distribution then can be used to identify the location and size of unknown lump during real-time abnormality detection procedure.

References

- [1] D. B. Camarillo, T. M. Krummel and J. K. Salisbury. Robotic technology in surgery: Past, present, and future. *The American Journal of Surgery* 188(4), pp. 2-15. 2004.
- [2] J. Dwivedi and I. Mahgoub. Robotic surgery—a review on recent advances in surgical robotic systems. Presented at Florida Conference on Recent Advances in Robotics. 2012, .
- [3] J. Li, Y. Xing, K. Liang and S. Wang. Kinematic design of a novel spatial remote center-of-motion mechanism for minimally invasive surgical robot. *Journal of Medical Devices* 9(1), pp. 011003. 2015.
- [4] A. Hamed, S. C. Tang, H. Ren, A. Squires, C. Payne, K. Masamune, G. Tang, J. Mohammadpour and Z. T. H. Tse. Advances in haptics, tactile sensing, and manipulation for robot-assisted minimally invasive surgery, noninvasive surgery, and diagnosis. *Journal of Robotics* 20122012.
- [5] K. J. Kuchenbecker. *Characterizing and Controlling the High-Frequency Dynamics of Haptic Interfaces* 2006.
- [6] J. Dargahi and S. Najarian. Human tactile perception as a standard for artificial tactile sensing—a review. *The International Journal of Medical Robotics and Computer Assisted Surgery* 1(1), pp. 23-35. 2004.
- [7] 2012, Robotic Surgery. <https://www.quora.com/Is-there-a-future-in-robotic-surgery-and-what-path-should-I-take-to-get-into-this-field>.
- [8] "OPERATION LINDBERGH", 2015, Websurg Websit. http://www.websurg.com/event/20010907_OperationLindbergh/Operation_Lindbergh.html.
- [9] A. M. Okamura. Haptic feedback in robot-assisted minimally invasive surgery. *Curr. Opin. Urol.* 19(1), pp. 102-107. 2009.
- [10] J. K. Kam, S. D. Cooray, J. K. Kam, J. A. Smith and A. A. Almeida. A cost-analysis study of robotic versus conventional mitral valve repair. *Heart, Lung and Circulation* 19(7), pp. 413-418. 2010.
- [11] M. R. Dylewski, A. C. Ohaeto and J. F. Pereira. Pulmonary resection using a total endoscopic robotic video-assisted approach. Presented at Seminars in Thoracic and Cardiovascular Surgery. 2011, .
- [12] J. Dargahi and S. Najarian. Advances in tactile sensors design/manufacturing and its impact on robotics applications-a review. *Industrial Robot: An International Journal* 32(3), pp. 268-281. 2005.

- [13] A. Hamed, S. C. Tang, H. Ren, A. Squires, C. Payne, K. Masamune, G. Tang, J. Mohammadpour and Z. T. H. Tse. Advances in haptics, tactile sensing, and manipulation for robot-assisted minimally invasive surgery, noninvasive surgery, and diagnosis. *Journal of Robotics* 20122012.
- [14] A. M. Okamura. Haptic feedback in robot-assisted minimally invasive surgery. *Curr. Opin. Urol.* 19(1), pp. 102-107. 2009.
- [15] M. Fontana, E. Ruffaldi, F. Salasedo and M. Bergamasco. On the integration of tactile and force feedback, haptics rendering and applications. 2012.
- [16] H. Aydin, K. Volkan and R. Ali. Identification and localization of prostate cancer with combined use of T2-weighted, diffusion weighted MRI and proton MR spectroscopy, correlation with histopathology. *Advances in Molecular Imaging* 3(03), pp. 23. 2013.
- [17] A. Karatopis, S. Anastasopoulos, S. Drakopoulos, M. Douskou, G. Panagiotakis and I. Kandarakis. Assessment and optimization of TEA-PRESS sequences in 1H MRS and MRSI of the breast. Presented at Imaging Systems and Techniques, 2008. IST 2008. IEEE International Workshop On. 2008, .
- [18] P. J. Edwards, D. L. Hill, J. A. Little and D. J. Hawkes. A three-component deformation model for image-guided surgery. *Med. Image Anal.* 2(4), pp. 355-367. 1998.
- [19] O. Ukimura. Image-guided surgery in minimally invasive urology. *Curr. Opin. Urol.* 20(2), pp. 136-140. 2010.
- [20] M. Hashizume. MRI-guided laparoscopic and robotic surgery for malignancies. *International Journal of Clinical Oncology* 12(2), pp. 94-98. 2007.
- [21] R. Gassert, A. Yamamoto, D. Chapuis, L. Dovat, H. Bleuler and E. Burdet. Actuation methods for applications in MR environments. *CONCEPTS IN MAGNETIC RESONANCE PART B MAGNETIC RESONANCE ENGINEERING* 29(4), pp. 191. 2006.
- [22] P. Mozer, J. Troccaz and D. Stoianovici. Urologic robots and future directions. *Curr. Opin. Urol.* 19(1), pp. 114-119. 2009.
- [23] D. Stoianovici, A. Patriciu, D. Petrisor, D. Mazilu and L. Kavoussi. A new type of motor: Pneumatic step motor. *Mechatronics, IEEE/ASME Transactions On* 12(1), pp. 98-106. 2007.
- [24] M. Muntener, A. Patriciu, D. Petrisor, D. Mazilu, H. Bagga, L. Kavoussi, K. Cleary and D. Stoianovici. Magnetic resonance imaging compatible robotic system for fully automated brachytherapy seed placement. *Urology* 68(6), pp. 1313-1317. 2006.
- [25] K. Masamune, E. Kobayashi, Y. Masutani, M. Suzuki, T. Dohi, H. Iseki and K. Takakura. Development of an MRI-compatible needle insertion manipulator for stereotactic neurosurgery. *Computer Aided Surgery* 1(4), pp. 242-248. 1995.

- [26] H. Elhawary, A. Zivanovic, B. Davies and M. Lamperth. A review of magnetic resonance imaging compatible manipulators in surgery. *Proc. Inst. Mech. Eng. H.* 220(3), pp. 413-424. 2006.
- [27] Y. Jiang, G. Li, L. Qian, X. Hu, D. Liu, S. Liang and Y. Cao. Characterization of the nonlinear elastic properties of soft tissues using the supersonic shear imaging (SSI) technique: Inverse method, ex vivo and in vivo experiments. *Med. Image Anal.* 20(1), pp. 97-111. 2015.
- [28] D. Nolan, A. Gower, M. Destrade, R. Ogden and J. McGarry. A robust anisotropic hyperelastic formulation for the modelling of soft tissue. *Journal of the Mechanical Behavior of Biomedical Materials* 39pp. 48-60. 2014.
- [29] H. Taghizadeh, M. Tafazzoli-Shadpour, M. B. Shadmehr and N. Fatourae. Evaluation of biaxial mechanical properties of aortic media based on the lamellar microstructure. *Materials* 8(1), pp. 302-316. 2015.
- [30] C. Basdogan. "Dynamic material properties of human and animal livers," in *Soft Tissue Biomechanical Modeling for Computer Assisted Surgery* Anonymous 2012, .
- [31] E. Samur, M. Sedef, C. Basdogan, L. Avtan and O. Duzgun. A robotic indenter for minimally invasive measurement and characterization of soft tissue response. *Med. Image Anal.* 11(4), pp. 361-373. 2007.
- [32] A. Hassanbeiglou, M. Kalantari, E. Mozaffari, J. Dargahi and J. Kövecses. A new tactile array sensor for viscoelastic tissues with time-dependent behavior. *Sens Rev* 35(4), pp. 374-381. 2015.
- [33] M. Kalantari, M. Ramezanifard, R. Ahmadi, J. Dargahi and J. Kövecses. A piezoresistive tactile sensor for tissue characterization during catheter-based cardiac surgery. *The International Journal of Medical Robotics and Computer Assisted Surgery* 7(4), pp. 431-440. 2011.
- [34] H. Xie, H. Liu, L. D. Seneviratne and K. Althoefer. An optical tactile array probe head for tissue palpation during minimally invasive surgery. *Sensors Journal, IEEE* 14(9), pp. 3283-3291. 2014.
- [35] M. P. Ottensmeyer, A. E. Kerdok, R. D. Howe and S. L. Dawson. "The effects of testing environment on the viscoelastic properties of soft tissues," in *Medical Simulation* Anonymous 2004, .
- [36] J. L. Taylor. "Kinesthetic inputs," in *Neuroscience in the 21st Century* Anonymous 2013, .
- [37] G. Robles-De-La-Torre and V. Hayward. Force can overcome object geometry in the perception of shape through active touch. *Nature* 412(6845), pp. 445-448. 2001.
- [38] A. M. Kappers. Human perception of shape from touch. *Philos. Trans. R. Soc. Lond. B. Biol. Sci.* 366(1581), pp. 3106-3114. 2011.

- [39] A. F. J. Sanders. *Investigations into Haptic Space and Haptic Perception of Shape for Active Touch* 2008.
- [40] V. Hayward, O. R. Astley, M. Cruz-Hernandez, D. Grant and G. Robles-De-La-Torre. Haptic interfaces and devices. *Sens Rev* 24(1), pp. 16-29. 2004.
- [41] G. A. Tabot, S. S. Kim, J. E. Winberry and S. J. Bensmaia. Restoring tactile and proprioceptive sensation through a brain interface. *Neurobiol. Dis.* 2014.
- [42] J. J. Craig. *Introduction to Robotics: Mechanics and Control* 20053.
- [43] K. O. Johnson. The roles and functions of cutaneous mechanoreceptors. *Curr. Opin. Neurobiol.* 11(4), pp. 455-461. 2001.
- [44] A. Pérez-González, M. Vergara and J. L. Sancho-Bru. Stiffness map of the grasping contact areas of the human hand. *J. Biomech.* 46(15), pp. 2644-2650. 2013.
- [45] A. W. Goodwin and H. E. Wheat. Sensory signals in neural populations underlying tactile perception and manipulation. *Annu. Rev. Neurosci.* 27pp. 53-77. 2004.
- [46] H. Liu, J. Li, X. Song, L. D. Seneviratne and K. Althoefer. Rolling indentation probe for tissue abnormality identification during minimally invasive surgery. *Robotics, IEEE Transactions On* 27(3), pp. 450-460. 2011.
- [47] K. Nichols and A. Okamura. A framework for multilateral manipulation in surgical tasks. Presented at The Hamlyn Symposium on Medical Robotics. 2014, .
- [48] "CRS Catalyst-5 Robot", 2014, Quanser Website.
http://www.quanser.com/Products/quarc/documentation/quarc_using_devices_robots.html#catalyst.
- [49] H. Yussof, M. Ohka, H. Suzuki, N. Morisawa and J. Takata. Control scheme of object manipulation based on tactile sensing in humanoid robot arm. 2007.
- [50] Q. Li, C. Schürmann, R. Haschke and H. Ritter. A control framework for tactile servoing. 2013.
- [51] D. P. Noonan, H. Liu, Y. H. Zwei, K. Althoefer and L. D. Seneviratne. A dual-function wheeled probe for tissue viscoelastic property identification during minimally invasive surgery. Presented at Robotics and Automation, 2007 IEEE International Conference On. 2007, .
- [52] M. Vatani, E. D. Engeberg and J. Choi. Detection of the position, direction and speed of sliding contact with a multi-layer compliant tactile sensor fabricated using direct-print technology. *Smart Mater. Struct.* 23(9), pp. 095008. 2014.

- [53] S. Denei, F. Mastrogiovanni and G. Cannata. Towards the creation of tactile maps for robots and their use in robot contact motion control. *Robotics and Autonomous Systems* 63pp. 293-308. 2015.
- [54] J. Wang and Y. Li. Surface-tracking of a 5-DOF manipulator equipped with tactile sensors. Presented at Control Automation Robotics & Vision (ICARCV), 2010 11th International Conference On. 2010, .
- [55] "3132-Micro Load Cell", 2015, Phidget Website.
http://www.phidgets.com/products.php?product_id=3132.
- [56] "Load Cell Primer", 2015, Phidget Website.
http://www.phidgets.com/docs/Load_Cell_Primer.
- [57] C. Passenberg, A. Peer and M. Buss. A survey of environment-, operator-, and task-adapted controllers for teleoperation systems. *Mechatronics* 20(7), pp. 787-801. 2010.
- [58] S. Najarian, J. Dargahi and A. Mehrizi. *Artificial Tactile Sensing in Biomedical Engineering* 2009.
- [59] S. Nicolle and J. Palierne. Dehydration effect on the mechanical behaviour of biological soft tissues: Observations on kidney tissues. *Journal of the Mechanical Behavior of Biomedical Materials* 3(8), pp. 630-635. 2010.
- [60] J. Konstantinova, M. Li, G. Mehra, P. Dasgupta, K. Althoefer and T. Nanayakkara. Behavioral characteristics of manual palpation to localize hard nodules in soft tissues. *Biomedical Engineering, IEEE Transactions On* 61(6), pp. 1651-1659. 2014.
- [61] X. Jiang, P. J. Scott, D. J. Whitehouse and L. Blunt. Paradigm shifts in surface metrology. part I. historical philosophy. Presented at Proceedings of the Royal Society of London A: Mathematical, Physical and Engineering Sciences. 2007, .
- [62] K. Captain, A. Boghani and D. Wormley. Analytical tire models for dynamic vehicle simulation. *Veh. Syst. Dyn.* 8(1), pp. 1-32. 1979.
- [63] H. Liu, D. P. Noonan, K. Althoefer and L. D. Seneviratne. Rolling mechanical imaging: A novel approach for soft tissue modelling and identification during minimally invasive surgery. Presented at Robotics and Automation, 2008. ICRA 2008. IEEE International Conference On. 2008, .
- [64] K. Sangpradit, H. Liu, L. D. Seneviratne and K. Althoefer. Tissue identification using inverse finite element analysis of rolling indentation. Presented at Robotics and Automation, 2009. ICRA'09. IEEE International Conference On. 2009, .

- [65] S. Lou, X. Jiang, P. J. Bills and P. J. Scott. Defining true tribological contact through application of the morphological method to surface topography. *Tribology Letters* 50(2), pp. 185-193. 2013.
- [66] X. J. Jiang and D. J. Whitehouse. Technological shifts in surface metrology. *CIRP Annals-Manufacturing Technology* 61(2), pp. 815-836. 2012.
- [67] G. H. Martin. *Kinematics and Dynamics of Machines* 2002.
- [68] "Circlefit3d - fit circle to three points in 3d space", 2012, J. Korsawe. <http://www.mathworks.com/matlabcentral/fileexchange/34792-circlefit3d-fit-circle-to-three-points-in-3d-space>;
- [69] K. Kanatani and P. Rangarajan. Hyper least squares fitting of circles and ellipses. *Comput. Stat. Data Anal.* 55(6), pp. 2197-2208. 2011.
- [70] A. Al-Sharadqah and N. Chernov. Error analysis for circle fitting algorithms. *Electronic Journal of Statistics* 3pp. 886-911. 2009.
- [71] "3D Laser Scanner, LPX-250", 2012, Roland Website. <http://www.rolanddg.com/product/archives/lpx-250/spec.html>.
- [72] I. Van den Herrewegen, K. Cuppens, M. Broeckx, B. Barisch-Fritz, J. Vander Sloten, A. Leardini and L. Peeraer. Dynamic 3D scanning as a markerless method to calculate multi-segment foot kinematics during stance phase: Methodology and first application. *J. Biomech.* 47(11), pp. 2531-2539. 2014.
- [73] H. M. Kjer and J. Wilm. *Evaluation of Surface Registration Algorithms for PET Motion Correction* 2010.
- [74] B. Li, A. Kidane, G. Ravichandran and M. Ortiz. Verification and validation of the optimal transportation meshfree (OTM) simulation of terminal ballistics. *Int. J. Impact Eng.* 42pp. 25-36. 2012.
- [75] G. R. Joldes, A. Wittek and K. Miller. Suite of finite element algorithms for accurate computation of soft tissue deformation for surgical simulation. *Med. Image Anal.* 13(6), pp. 912-919. 2009.
- [76] A. C. Fischer-Cripps and I. Mustafaev. *Introduction to Contact Mechanics* 2000.
- [77] Y. Fung. *Biomechanics: Mechanical Properties of Living Tissues* 2013.
- [78] A. M. Okamura, C. Simone and M. Leary. Force modeling for needle insertion into soft tissue. *Biomedical Engineering, IEEE Transactions On* 51(10), pp. 1707-1716. 2004.

- [79] D. Placko and T. Kundu. *Advanced Ultrasonic Methods for Material and Structure Inspection* 2013.
- [80] I. B. Wanninayake, P. Dasgupta, L. D. Seneviratne and K. Althoefer. Air-float palpation probe for tissue abnormality identification during minimally invasive surgery. *Biomedical Engineering, IEEE Transactions On* 60(10), pp. 2735-2744. 2013.
- [81] J. D. Brown, J. Rosen, Y. S. Kim, L. Chang, M. N. Sinanan and B. Hannaford. In-vivo and in-situ compressive properties of porcine abdominal soft tissues. *Stud. Health Technol. Inform.* pp. 26-32. 2003.
- [82] K. Tan, S. Cheng, L. Jugé and L. E. Bilston. Characterising soft tissues under large amplitude oscillatory shear and combined loading. *J. Biomech.* 46(6), pp. 1060-1066. 2013.
- [83] R. Reiter, C. Freise, K. Jöhrens, C. Kamphues, D. Seehofer, M. Stockmann, R. Somasundaram, P. Asbach, J. Braun and A. Samani. Wideband MRE and static mechanical indentation of human liver specimen: Sensitivity of viscoelastic constants to the alteration of tissue structure in hepatic fibrosis. *J. Biomech.* 47(7), pp. 1665-1674. 2014.
- [84] M. Ayyildiz, S. Cinoglu and C. Basdogan. Effect of normal compression on the shear modulus of soft tissue in rheological measurements. *Journal of the Mechanical Behavior of Biomedical Materials* 2015.
- [85] B. Yarpuzlu, M. Ayyildiz, O. E. Tok, R. G. Aktas and C. Basdogan. Correlation between the mechanical and histological properties of liver tissue. *Journal of the Mechanical Behavior of Biomedical Materials* 29pp. 403-416. 2014.
- [86] S. Ocal, M. U. Ozcan, I. Basdogan and C. Basdogan. Effect of preservation period on the viscoelastic material properties of soft tissues with implications for liver transplantation. *J. Biomech. Eng.* 132(10), pp. 101007. 2010.
- [87] V. Egorov, S. Tsyuryupa, S. Kanilo, M. Kogit and A. Sarvazyan. Soft tissue elastometer. *Med. Eng. Phys.* 30(2), pp. 206-212. 2008.
- [88] D. O. Recouvreux, C. R. Rambo, F. V. Berti, C. A. Carminatti, R. V. Antônio and L. M. Porto. Novel three-dimensional cocoon-like hydrogels for soft tissue regeneration. *Materials Science and Engineering: C* 31(2), pp. 151-157. 2011.
- [89] A. M. Okamura. Haptic feedback in robot-assisted minimally invasive surgery. *Curr. Opin. Urol.* 19(1), pp. 102-107. 2009.
- [90] J. Dargahi and S. Najarian. Advances in tactile sensors design/manufacturing and its impact on robotics applications-a review. *Industrial Robot: An International Journal* 32(3), pp. 268-281. 2005.

- [91] J. Dargahi, S. Sokhanvar, S. Najarian and S. Arbatani. *Tactile Sensing and Display: Haptic Feedback for Minimally Invasive Surgery and Robotics* 2012.
- [92] S. Najarian, J. Dargahi, G. Darbemamieh and S. H. Farkoush. *Mechatronics in Medicine A Biomedical Engineering Approach* 2011.
- [93] J. M. Romano, K. Hsiao, G. Niemeyer, S. Chitta and K. J. Kuchenbecker. Human-inspired robotic grasp control with tactile sensing. *Robotics, IEEE Transactions On* 27(6), pp. 1067-1079. 2011.
- [94] A. Ataollahi, P. Polygerinos, P. Puangmali, L. D. Seneviratne and K. Althoefer. Tactile sensor array using prismatic-tip optical fibers for dexterous robotic hands. Presented at Intelligent Robots and Systems (IROS), 2010 IEEE/RSJ International Conference On. 2010, .
- [95] A. Schmitz, P. Maiolino, M. Maggiali, L. Natale, G. Cannata and G. Metta. Methods and technologies for the implementation of large-scale robot tactile sensors. *Robotics, IEEE Transactions On* 27(3), pp. 389-400. 2011.
- [96] R. S. Dahiya, G. Metta, M. Valle and G. Sandini. Tactile sensing—from humans to humanoids. *Robotics, IEEE Transactions On* 26(1), pp. 1-20. 2010.
- [97] R. S. Dahiya, G. Metta and M. Valle. Development of fingertip tactile sensing chips for humanoid robots. Presented at Mechatronics, 2009. ICM 2009. IEEE International Conference On. 2009, .
- [98] N. Sommer and A. Billard. Face classification using touch with a humanoid robot hand. Presented at Humanoid Robots (Humanoids), 2012 12th IEEE-RAS International Conference On. 2012, .
- [99] T. L. Chen, C. A. King, A. L. Thomaz and C. C. Kemp. An investigation of responses to robot-initiated touch in a nursing context. *International Journal of Social Robotics* 6(1), pp. 141-161. 2014.
- [100] S. Yohanan and K. E. MacLean. The haptic creature project: Social human-robot interaction through affective touch. Presented at Proceedings of the AISB 2008 Symposium on the Reign of Catz & Dogs: The Second AISB Symposium on the Role of Virtual Creatures in a Computerised Society. 2008, .
- [101] R. S. Dahiya, D. Cattin, A. Adami, C. Collini, L. Barboni, M. Valle, L. Lorenzelli, R. Oboe, G. Metta and F. Brunetti. Towards tactile sensing system on chip for robotic applications. *Sensors Journal, IEEE* 11(12), pp. 3216-3226. 2011.
- [102] S. Aoyagi, T. Matsuda, T. Kong, T. Ishimaru, M. Suzuki and K. Inoue. Proposal and development of arrayed sole sensor for legged robot and contact force detection using neural networks. *Sensors Journal, IEEE* 11(9), pp. 2048-2056. 2011.

- [103] F. Adams and A. J. Brock. *Hippocratic Writings* 1955.
- [104] C. Filloy, H. Roham, S. Najarian, S. Mohsen Hosseini and J. Dargahi. Design and fabrication of a new tactile probe for measuring the modulus of elasticity of soft tissues. *Sens Rev* 27(4), pp. 317-323. 2007.
- [105] M. Ayyildiz, B. Guclu, M. Z. Yildiz and C. Basdogan. An optoelectromechanical tactile sensor for detection of breast lumps. *Haptics, IEEE Transactions On* 6(2), pp. 145-155. 2013.
- [106] S. Stassi, V. Cauda, G. Canavese and C. F. Pirri. Flexible tactile sensing based on piezoresistive composites: A review. *Sensors* 14(3), pp. 5296-5332. 2014.
- [107] S. Stassi. *Tactile Sensor Devices Exploiting the Tunnelling Conduction in Piezoresistive Composites* 2013.
- [108] V. Maheshwari and R. F. Saraf. High-resolution thin-film device to sense texture by touch. *Science* 312(5779), pp. 1501-1504. 2006.
- [109] M. I. Tiwana, S. J. Redmond and N. H. Lovell. A review of tactile sensing technologies with applications in biomedical engineering. *Sensors and Actuators A: Physical* 179pp. 17-31. 2012.
- [110] M. Kalantari. *Development of Piezoresistive Tactile Sensors and a Graphical Display System for Minimally Invasive Surgery and Robotics* 2013.
- [111] J. D. Brown, J. Rosen, Y. S. Kim, L. Chang, M. N. Sinanan and B. Hannaford. In-vivo and in-situ compressive properties of porcine abdominal soft tissues. *Stud. Health Technol. Inform.* pp. 26-32. 2003.
- [112] J. Dargahi, S. Arbatani, S. Sokhanvar, W. Xie and R. Ramezanifard. A novel tactile softness display for minimally invasive surgery. *Mechatronics* 24(8), pp. 1144-1156. 2014.
- [113] K. Nichols and A. M. Okamura. Methods to segment hard inclusions in soft tissue during autonomous robotic palpation. *Robotics, IEEE Transactions On* 31(2), pp. 344-354. 2015.